RESEARCH ARTICLE

Multifaceted actions of Zeb2 in postnatal neurogenesis from the ventricular-subventricular zone to the olfactory bulb

Astrid Deryckere[1,¶], Elke Stappers[2,3,¶], Ruben Dries[2,3,*], Elise Peyre[4], Veronique van den Berghe[2,5], Andrea Conidi[3], F. Isabella Zampeta[3], Annick Francis[2], Marjolein Bresseleers[2], Agata Stryjewska[2,‡], Ria Vanlaer[1], Elke Maas[6,§], Ihor V. Smal[3,7], Wilfred F. J. van IJcken[3,8], Frank G. Grosveld[3], Laurent Nguyen[4], Danny Huylebroeck[2,3,**] and Eve Seuntjens[1,2,**,‡‡]

ABSTRACT

The transcription factor Zeb2 controls fate specification and subsequent differentiation and maturation of multiple cell types in various embryonic tissues. It binds many protein partners, including activated Smad proteins and the NuRD co-repressor complex. How Zeb2 subdomains support cell differentiation in various contexts has remained elusive. Here, we studied the role of Zeb2 and its domains in neurogenesis and neural differentiation in the young postnatal ventricular-subventricular zone (V-SVZ), in which neural stem cells generate olfactory bulb-destined interneurons. Conditional *Zeb2* knockouts and separate acute loss- and gain-of-function approaches indicated that Zeb2 is essential for controlling apoptosis and neuronal differentiation of V-SVZ progenitors before and after birth, and we identified *Sox6* as a potential downstream target gene of Zeb2. *Zeb2* genetic inactivation impaired the differentiation potential of the V-SVZ niche in a cell-autonomous fashion. We also provide evidence that its normal function in the V-SVZ also involves non-autonomous mechanisms. Additionally, we demonstrate distinct roles for Zeb2 protein-binding domains, suggesting that Zeb2 partners co-determine neuronal output from the mouse V-SVZ in both quantitative and qualitative ways in early postnatal life.

KEY WORDS: Postnatal neurogenesis, NuRD, Olfactory bulb, Smad, Ventricular-subventricular zone, Zeb2

[1]Laboratory of Developmental Neurobiology, Department of Biology, KU Leuven, Leuven 3000, Belgium. [2]Laboratory of Molecular Biology (Celgen), Department of Development and Regeneration, KU Leuven, Leuven 3000, Belgium. [3]Department of Cell Biology, Erasmus University Medical Center, Rotterdam 3015 CN, The Netherlands. [4]GIGA-Stem Cells and GIGA-Neurosciences, Liège University, Liège 4000, Belgium. [5]Department of Developmental Neurobiology, Institute of Psychiatry, Psychology and Neuroscience, and MRC Centre for Neurodevelopmental Disorders, King's College London, London SE1 1UL, UK. [6]Department of Cardiovascular Sciences, Center for Molecular and Vascular Biology, KU Leuven, Leuven 3000, Belgium. [7]Department of Molecular Genetics, Erasmus University Medical Center, Rotterdam 3015 CN, The Netherlands. [8]Center for Biomics-Genomics, Department of Cell Biology, Erasmus University Medical Center, Rotterdam 3015 CN, The Netherlands.
*Present address: Department of Medicine, Harvard Medical School, and Department of Medical Oncology, Dana-Farber Cancer Institute, Boston, MA 02115, USA. ‡Present address: Neural Development, Plasticity and Repair, Wolfson Institute for Biomedical Research, University College London, London WC1E 6BT, UK. §Present address: Laboratory of Virology and Chemotherapy (Rega Institute), KU Leuven, Leuven 3000, Belgium.
¶These authors contributed equally to this work
**These authors contributed equally to this work

‡‡Author for correspondence (eve.seuntjens@kuleuven.be)

E.Stappers, 0000-0002-9589-8057; E.P., 0000-0002-4737-1306; M.B., 0000-0003-0371-1644; D.H., 0000-0003-4862-1079; E.Seuntjens, 0000-0002-0126-461X

INTRODUCTION

Neurogenesis in the central nervous system starts during embryonic development and continues after birth in two discrete regions of the mammalian brain: the subgranular zone (SGZ) of the hippocampal dentate gyrus and the ventricular-subventricular zone (V-SVZ) lining the lateral ventricle walls. In rodents, newly formed SGZ neurons integrate locally, whereas V-SVZ neuroblasts migrate over a long distance before integrating and maturing in the olfactory bulb (OB) (Altman, 2011; Lim and Alvarez-Buylla, 2014; Urbán and Guillemot, 2014).

The postnatal neurogenic zones have an embryonic origin. In the case of the V-SVZ, a fraction of forebrain radial glial cells (RGCs) in the lateral ganglionic eminences (LGEs) and pallium becomes quiescent (Young et al., 2007; Fuentealba et al., 2015). These progenitor cells are reactivated early after birth and differentiate into either supportive niche-regulatory ependymal cells or radial glial-like neural stem cells (NSCs or B1 cells) of the V-SVZ (Mirzadeh et al., 2008; Fuentealba et al., 2015). These B1 cells proliferate slowly and generate transit-amplifying cells (C cells), which in turn give rise to immature migratory neuroblasts (A cells). Neuroblasts migrate via the rostral migratory stream (RMS) towards the OB where they disperse radially, and eventually mature into network-integrated periglomerular or granular interneurons (Doetsch and Alvarez-Buylla, 1996; Doetsch et al., 1997; Alvarez-Buylla and García-Verdugo, 2002; Bjornsson et al., 2015; Lim and Alvarez-Buylla, 2016). In addition to these GABAergic interneurons, the OB contains glutamatergic tufted and mitral cells, as well as juxtaglomerular interneurons (Blanchart et al., 2006; Brill et al., 2010; Díaz-Guerra et al., 2013).

Interneuron diversity in the OB is achieved through a combination of temporal and regional controls, whereby proliferating NSCs generate distinct populations of OB interneurons at different time points (Lemasson et al., 2005; Batista-Brito et al., 2008b). Neurons born in the first postnatal week are more prone to become superficial granule cells compared with cells born later (Lemasson et al., 2005). Furthermore, extrinsic and intrinsic factors, epigenetic and transcriptional controls, and apoptosis influence OB interneuron production, fate specification and maturation (reviewed by Díaz-Guerra et al., 2013; Lim and Alvarez-Buylla, 2016).

Zeb2 (Sip1, Zfhx1b) is a DNA-binding transcription factor that binds E-box-like sequences in gene regulatory regions (Remacle et al., 1999; Verschueren et al., 1999). In humans, *de novo* mutation of one *ZEB2* allele causes Mowat-Wilson Syndrome (MOWS; OMIM #235730) (Mowat et al., 1998; Cacheux et al., 2001; Wakamatsu et al., 2001), whereas mutations in *ZEB1*, the second member of this family, cause corneal dystrophy in the eye (Chung et al., 2014). MOWS is a severe developmental disorder affecting both the neural crest and neural lineages. It is characterized by

DEVELOPMENT

typical impediments of craniofacial development, severe intellectual disability in most individuals, and, in many cases, epilepsy and Hirschsprung disease (Zweier et al., 2002, 2005; Garavelli and Mainardi, 2007; Ivanovski et al., 2018).

Murine Zeb2 is 1215 amino acids long and structurally similar to Zeb1 (δEF1, Zfhx1a) (Funahashi et al., 1991). Both have two separated clusters of zinc fingers [the N- and C-terminal zinc finger domains (NZF and CZF, respectively)] wherein the two last fingers each bind predominantly to 5′-CACCT(G) on target DNA (Sekido et al., 1994; Remacle et al., 1999). Zeb2 NZF and CZF domains are separated by a Smad-binding domain (SBD) and, similar to Zeb1, a non-DNA-binding homeodomain-like domain (HD) and a domain facilitating the interaction with Ctbp1/2 co-repressors [CtBP-interacting domain (CID)]. Both Zeb proteins also contain a short motif [designated as the nucleosome remodeling and deacetylation complex (NuRD) interaction motif (NIM)], located close to the N-terminus, that enables binding to NuRD (Verschueren et al., 1999; Van Grunsen et al., 2001; Verstappen et al., 2008; Conidi et al., 2011, 2013). In individuals with MOWS, ~300 ZEB2 genetic mutations have been mapped so far. Most mutations lead to a C-terminal truncated unstable protein (Zweier et al., 2005; Garavelli et al., 2009; Ivanovski et al., 2018). However, some missense or in-frame deletion mutations in ZEB2 protein-encoding exons have been described, which usually lead to a milder form of MOWS (Yoneda et al., 2002; Gregory-Evans et al., 2004; Zweier et al., 2005, 2006; Heinritz et al., 2006). For example, mutations disrupting a splice site affecting the interaction of ZEB2 with NuRD cause a mild form of MOWS, associated with fewer psychomotor developmental difficulties or less striking facial gestalt, as well as the absence of other anomalies, such as agenesis of the corpus callosum and heart defects (Yoneda et al., 2002; Zweier et al., 2006; Verstappen et al., 2008).

Conditional, cell-type-specific Zeb2 knockouts (cKOs) in the mouse have improved the understanding of MOWS-related neurodevelopmental defects (reviewed by Conidi et al., 2011; Hegarty et al., 2015). During cortical development, Zeb2 directs the proper timing of neurogenesis and gliogenesis, and is essential for the guided migration of ventral forebrain-born cortical interneurons (Seuntjens et al., 2009; McKinsey et al., 2013; van den Berghe et al., 2013). Correct cortical interneuron migration requires intact zinc-finger (ZnF) and SBD domains in Zeb2 (Conidi et al., 2013).

Although it has been shown that reduced levels of micro-RNAs of the miR-200 cluster induced Zeb2 expression and premature differentiation of OB interneurons (Beclin et al., 2016), the precise role of Zeb2 (and its domains) in postnatal neurogenesis and OB interneuron maturation remains unknown. Here, using a combination of Cre-dependent Zeb2 cKO, and acute loss- versus gain-of-function approaches, we show that Zeb2 controls the numerical output from the V-SVZ, as well as differentiation of OB interneurons. Intriguingly, non-Cre-targeted cells also display phenotypes in both processes, indicating that Zeb2 acts partly in a non-cell-autonomous fashion. RNA-seq, ChIP and functional analysis identified Sox6 as a target of Zeb2. Rescue experiments using domain mutants of Zeb2 in cKO settings differentially affected OB interneuron development. Hence, Zeb2 integrates diverse signals and teams up with different partner proteins in the young postnatal V-SVZ niche in order to steer OB interneuron development.

RESULTS
Knockout of Zeb2 in the embryonic LGE severely disrupts development of the OB
At the time when B cells are set aside in the embryonic brain, Zeb2 mRNA/protein is present in the ventral telencephalon (van den

Berghe et al., 2013), including the LGE, which is the major source of B cells for the postnatal V-SVZ (Kriegstein and Alvarez-Buylla, 2009) (Fig. S1A). Zeb2 protein persists in the embryonic and early postnatal (P)5 and P18 V-SVZ (Fig. S1B-D). In embryonic day (E)16.5 and postnatal OBs, Zeb2 was detected throughout the granule cell layers (GCLs) and periglomerular layer (PGL) (Fig. S1E-H), but not in the mitral and external tufted cells, supported by the absence of Zeb2 and reelin co-staining in the P5 OB (Fig. S1I,Ia) (Hack et al., 2002; Okuyama-Yamamoto et al., 2005).

Zeb2 levels were high in the V-SVZ, as well as in OB interneurons, but lower in the migrating neuroblasts in the RMS (Fig. 1A-B). In the niche, Zeb2 was nearly absent from GFAP$^+$ B cells and appeared in EGFR$^+$ C cells and doublecortin$^+$ (Dcx$^+$) A cells (Fig. 1C-E). These expression patterns demonstrate an upregulation of Zeb2 upon maturation and suggest a dual role for Zeb2 in OB interneuron generation and differentiation.

We used Gsh2-Cre mice to inactivate Zeb2 in the LGE RGCs and their progeny, targeting a large proportion (~70%) of postnatal V-SVZ cells (Stenman et al., 2003; Kessaris et al., 2006; Young et al., 2007; van den Berghe et al., 2013). The Zeb2-floxed mouse line was first crossed with Cre-dependent GFP-reporter mice (RCE mice) to trace Zeb2-KO cells. We confirmed Zeb2 removal from the LGE at E14.5 in Zeb2cKO|Gsh2 mice (Fig. 1F,G; for strain designations, see Materials and Methods) in the V-SVZ at P2 using RNA-seq on fluorescence-activated cell-sorted (FACS) cells (Fig. S2A) and in tissue sections at P5 (Fig. S3A,B). We also ruled out the possibility of inefficient recombination to produce GFP in the Zeb2cKO|Gsh2 V-SVZ, because this could lead to an overestimation of non-cell-autonomous actions of Zeb2 (Fig. S3C). LGE-specific Zeb2 removal had a major impact on OB development. Fewer Zeb2-KO interneurons were found in the OB, in which they failed to distribute over the whole OB and instead clustered in the deep primitive GCLs and later on also around the intermediate plexiform layer (IPL) and mitral cell layer (MCL) (Fig. 1H-K), disturbing the development of the mitral cell layer (Fig. S4). At P17-P18, the mean area of the cross-sections of Zeb2cKO|Gsh2 OBs was 70% smaller, and the OB morphology was more rounded when compared with controls (Fig. 1L,M).

Zeb2 regulates neurogenic output to the OB in the young postnatal V-SVZ
The observed deterioration of the OBs was indicative of a prominent role of Zeb2 in postnatal neurogenesis. Hence, we conducted further analyses of the OBs at P5, when they display a very pronounced phenotype. To assess whether the reduction of OB size in Zeb2cKO|Gsh2 brains was due to decreased numbers of neuroblasts arriving in the OB, we quantified the number of Dcx$^+$ neuroblasts using Dcx mean fluorescence intensity measurements and found a significant decrease in Zeb2cKO|Gsh2 OBs compared with controls (Fig. 1N). Furthermore, the ratio of Dcx$^+$/GFP$^+$ neuroblasts in Zeb2cKO|Gsh2 OBs was 25% smaller than controls (Fig. 1O), suggesting that fewer neuroblasts arrived in the OB.

This reduction in neuroblast numbers in the KOs could arise from the misrouting of interneurons before their entrance into the OB or from their decreased production and/or survival in the V-SVZ. We tested this by in vivo electroporation of a TdTomato-encoding vector into the Zeb2cKO|Gsh2 and control V-SVZ at P2. Quantification of TdTomato$^+$ cells in the OB at P9 ensured expression of the construct in the V-SVZ and enabled the tracing of cells derived from the young postnatal niche to the OB (Fig. 2A). We found a drastic reduction in the number of TdTomato$^+$ cells that had arrived in the
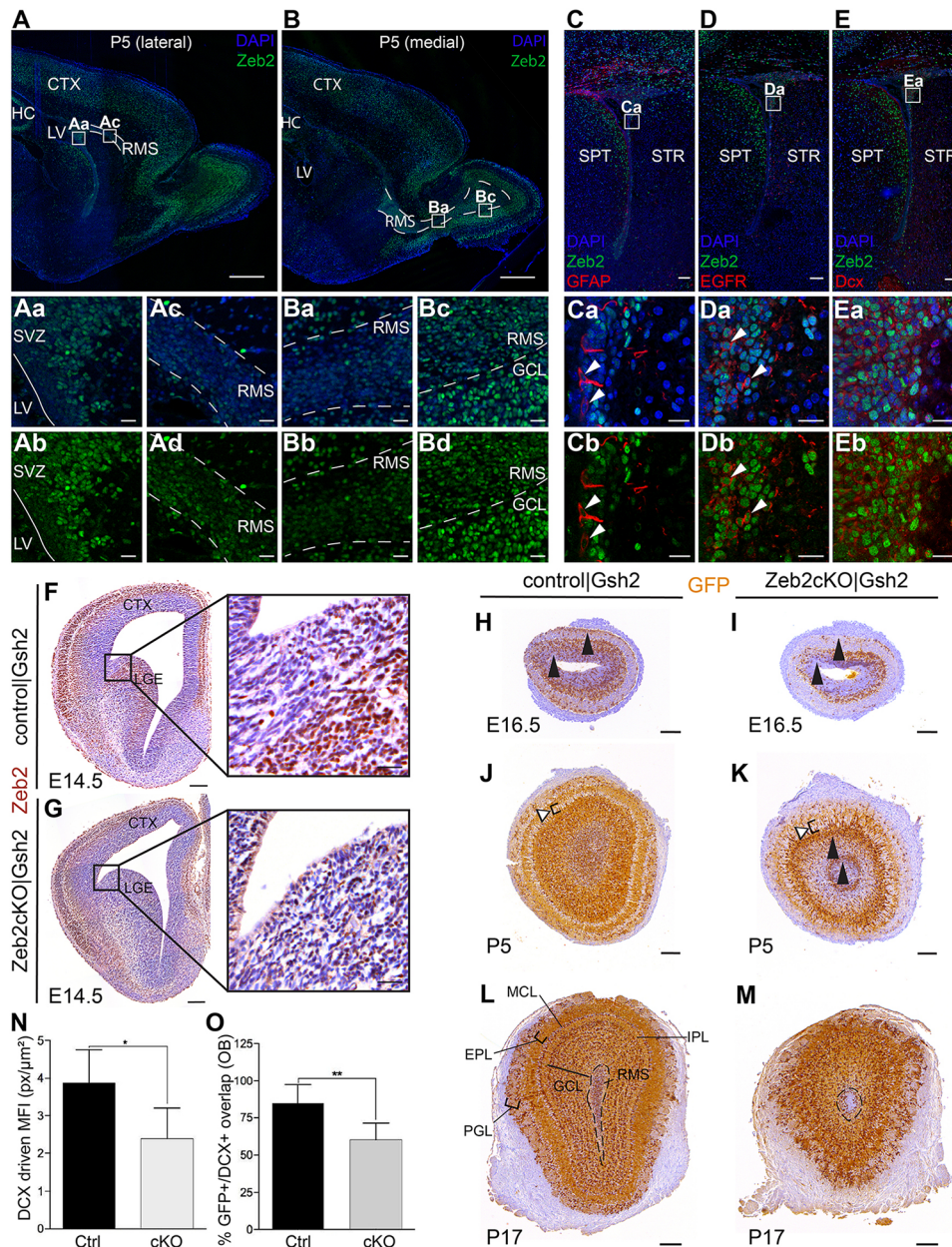
2

Fig. 1. Zeb2 is more prominent in differentiated cells, and its genetic inactivation impairs V-SVZ neuroblast output and OB organization.
(A-B) Zeb2 immunostaining on wild-type sagittal sections through the telencephalon at P5 with dashed lines indicating the RMS borders. Zeb2 levels were high in the V-SVZ (Aa), reduced in migrating neuroblasts in the RMS (Ac,Ba) and increased again in differentiated neurons in the GCL and PGL (Bc) (sections stained in one batch and imaged with the same settings). (C-E) Zeb2 and GFAP (C-Cb), EGFR (D-Db) or Dcx (E-Eb) co-staining on wild-type coronal sections at P5. Arrowheads indicate marker-positive cells and serve as a guide. Zeb2 levels were low in GFAP^{+} B cells and were upregulated in EGFR^{+} C cells and Dcx^{+} A cells (sections stained in one batch and imaged with the same settings for Zeb2). (F,G) Validation of Cre-mediated inactivation of Zeb2 in the Gsh2 model using immunostaining for Zeb2 on coronal E14.5 control|Gsh2 (F) and Zeb2cKO|Gsh2 (G) sections. (H-M) GFP immunohistochemistry showing Gsh2-Cre-targeted cells in control and *Zeb2* mutant OBs. (H,I) At E16.5, *Zeb2*-KO interneurons cluster together and fail to populate the outer developing GCL (arrowheads). (J,K) At P5, the GCLs were nearly depleted of GFP[+] (*Zeb2*-KO) cells when compared with controls. Targeted cells cluster in two ring-like structures in the mutant compared with control OBs (closed arrowheads). The RMS was almost depleted of targeted cells in mutant OBs, and their MCL did not mature in a tightly organized two- or three-cell thick layer (open arrowheads, MCL in brackets). (L,M) At P17, the Zeb2cKO|Gsh2 OB is rounder and the mean cross-section area was 70% smaller (*P*<0.01; mean areas: KO=1.68 mm[2]; control=2.42 mm[2]). Although GFP^{+} cells were distributed evenly in the GCLs, the typical layered GCL structure was visibly impaired. Furthermore, the IPL appeared to be invaded by GFP^{+} cells, whereas normally only a few cell bodies are found there. Mitral cells failed to form a smooth, single-cell layer. Dashed lines indicate the RMS-GCL border. (N) DCX-driven MFI in OBs at P5. The MFI was significantly reduced in the Zeb2cKO|Gsh2 versus control|Gsh2 OBs (2.4±0.40 versus 3.9±0.44 pixels/µm[2], respectively, two-tailed unpaired Student's *t*-test, *P<0.05, n=4). (O) GFP-Dcx overlap in OBs at P5, highlighting significant reduction in Zeb2cKO|Gsh2 versus control|Gsh2 OBs (85.1±5.5% versus 60.1±5.0%, respectively, two-tailed unpaired Student's *t*-test, **P<0.01, n=5). Data are mean±s.e.m. CTX, cortex; Dcx, doublecortin; EGFR, epidermal growth factor receptor; EPL, external plexiform layer; GCL, granule cell layer; GFAP, glial fibrillary acidic protein; HC, hippocampus; IPL, internal plexiform layer; LGE, lateral ganglionic eminence; LV, lateral ventricle; MCL, mitral cell layer; OB, olfactory bulb; PGL, periglomerular layer; RMS, rostral migratory stream; SPT, septum; STR, striatum; SVZ, subventricular zone. Scale bars: 500 µm (A,B); 100 µm (C-M); 20 µm in the magnified boxes (Aa-Eb, insets in F,G).

Zeb2cKO|Gsh2 OB (Fig. 2B-D). Furthermore, we could not find accumulations of TdTomato^{+} cells in the V-SVZ or RMS at P9 in Zeb2cKO|Gsh2 mice. In addition, no electroporated cells were found in other regions of the telencephalon, suggesting that the migratory route of these neuroblasts was not impaired. Remarkably, Zeb2-depleted cells within the OB looked morphologically aberrant: whereas control cells were bipolar with a leading process that oriented radially away from the RMS, Zeb2-depleted cells had a stunted shape and appeared disorganized (Fig. 2Ba,Ca). In particular, we measured the length of the leading process in Zeb2-KO interneurons in the GCL and found that it was 44% shorter than controls (Fig. 2E). In the Zeb2-cKO OBs, the number of cells without neurite extension also increased by 30%, whereas those with one neurite or one branched neurite decreased by 20% and 13%, respectively (Fig. 2F). This suggests that Zeb2 is important for the differentiation and maturation of OB interneurons.

To disentangle the embryonic from postnatal neurogenic actions of Zeb2, we acutely inactivated Zeb2 (by electroporation of a CAGGS-driven Cre-vector) in Zeb2[fl|ko] and control brains. Notably, in this setup, Zeb2 is depleted from a cohort of cells in the young postnatal V-SVZ that had developed normally, and cells become traceable via Cre-controlled GFP production. We found a similar drastic drop of Zeb2-KO neuron numbers in the OB (Fig. 2G-I), comparable with embryonic inactivation, and Zeb2-depleted OB interneurons showed a stunted shape and also appeared disorganized (Fig. 2Ga,Ha). To assess whether Zeb2-depleted neuroblasts might have arrived at a later time point in vivo, we electroporated Cre-vectors in the V-SVZ at P2 and assessed the number of targeted cells at P56 (i.e. 54 days post electroporation) (Fig. S5A). At this late stage too, significantly fewer GFP^{+} cells were found in Zeb2cKO|WT compared with control|WT OBs (Fig. S5B,C), suggesting that delayed migration cannot explain the phenotype. Collectively, these results suggest that Zeb2 has an essential cell-intrinsic stimulatory role in regulating the neurogenic output from the early-postnatal V-SVZ.

Zeb2 controls cell survival in the V-SVZ and olfactory bulb
As Zeb2 levels increase upon progression from NSC to neuroblast in the V-SVZ, we investigated whether Zeb2 acts primarily in B cells, or rather in C or A cells. In order to do this, we crossed Zeb2;RCE-floxed mice with a Dlx5/6-Cre line, which targets C and A cells in the ganglionic eminences (Stenman et al., 2003; van den Berghe et al., 2013). Notably, perinatal lethality of these mice prevents analysis of the phenotype beyond birth (see also van den Berghe et al., 2013). Nevertheless, at E18.5, when V-SVZ-derived interneurons are already detectable in the OB, the phenotype caused by the loss of Zeb2 was indistinguishable from the B cell targeting Gsh2-Cre Zeb2-cKO (Fig. S6A-D), suggesting that Zeb2 mainly acts in C cells and their progeny.

Given the pronounced decreased OB output, we next assessed cell proliferation in both Gsh2 and Dlx5/6 models in the V-SVZ at E18.5. We did not observe any differences in the number of phospho-histone H3 positive (PH3^{+}, G2/M phase) cells in the E18.5 V-SVZ in the Gsh2 model (Fig. S7A-D) or in the Dlx5/6 model (Fig. S7E). The situation was different in the postnatal V-SVZ in which, in the absence of Zeb2, the number of proliferating (Ki67^{+}) cells was reduced, but solely in cells not targeted by Gsh2-Cre (Fig. S7F-I). In order to address postnatal effects only, we used the acute deletion paradigm and analyzed proliferation in the V-SVZ at P5. Again, we did not observe a difference in the number of proliferating (Ki67^{+}) targeted cells (Fig. S7J-L). Taken together, our data suggest that there is no overt cell-autonomous proliferation defect in the absence of Zeb2 during postnatal neurogenesis.

Another mechanism that could explain the reduction in OB interneurons in the absence of Zeb2 is increased apoptosis. Therefore, we quantified the number of cleaved caspase 3 (CC3)-positive cells in the P5 V-SVZ and OB. We found a threefold increase in CC3^{+} cells in the Zeb2cKO|Gsh2 V-SVZ and a twofold increase in the OB compared with the control (Fig. 3A-F), indicating that Zeb2 promotes the survival of OB interneurons at different developmental phases.

Genetic inactivation of Zeb2 affects the maturation of various OB interneuron cell types
Considering the impact of Zeb2-KO on the morphology of OB interneurons, we next tested whether Zeb2-KO affected all types of OB interneuron or only specific subpopulations. Periglomerular cells in the OB include three major classes of dopaminergic interneuron: tyrosine hydroxylase-positive (TH[+]), calbindin-positive (CB[+]) and calretinin-positive (Calb2^{+}) cells (Kosaka et al., 1998). In addition, the soma of parvalbumin-positive (PV^{+}) cells are located in the external plexiform layer (EPL). The oncofetal trophoblast glycoprotein 5T4 is present in a specific subtype of OB granule cells found in the GCL and MCL, and regulates dendritic arborisation (Batista-Brito et al., 2008b; Yoshihara et al., 2012; Takahashi et al., 2016). We quantified these Calb2^{+}, CB[+], PV[+], 5T4[+] and TH[+] interneurons in OBs at P18. This is close to the age at which most Zeb2cKO|Gsh2 mice die but when expression of the OB interneuron markers is already well established. We found an overall decrease in each of these subtypes, with the exception of Calb2^{+} cells in Zeb2cKO|Gsh2 OBs, when compared with the control (Fig. 4). Intriguingly, we also observed a decrease in Cre-targeted cells (GFP[+]), as well as non-targeted (GFP^{−}) cells, upon Zeb2-cKO for 5T4, CB and PV subtypes (Fig. 4D-I,M-O). Remarkably, non-targeted PV[+] interneurons of Zeb2cKO|Gsh2 mice were improperly confined within the boundaries of the RMS in the OB (1% of PV^{+} cells in control versus 43% in cKO, P<0.01; Fig. 4M,N). We conclude that Zeb2-cKO affects the differentiation of most, but not all, OB interneuron subtypes in both cell- and non-cell-autonomous ways.

Upregulation of Sox6 in Zeb2-depleted cells is an important cause of defective OB interneuron development
To gain more insight into how Zeb2 normally controls the generation of early postnatal V-SVZ progenitors, we compared transcriptomes of Zeb2cKO|Gsh2 versus control V-SVZ cells after FACS. The respective samples clustered in two highly different groups (Fig. S2B). Principal component analysis (Fig. S2C) showed that they cluster together according to the first principal component (PC1).

Sox6 stood out in the RNA-seq analysis in the Zeb2cKO|Gsh2 V-SVZ as the most upregulated (4.6-fold) gene encoding a transcription factor. Sox6 steers cortical interneuron development and diversification, and is normally found in postmitotic cells of the embryonic ventral telencephalon (Azim et al., 2009; Batista-Brito et al., 2009). In the Zeb2cKO|Gsh2, we found a significant increase of Sox6 signal in GFP[+], as well as GFP^{−} cells within the entire V-SVZ (Fig. 5A-C). RT-qPCR analyses with independent samples confirmed a fourfold upregulation of Sox6 steady-state mRNA in Zeb2-mutant V-SVZ cells [average fold change=4.185 (n=3 for control and n=2 for cKO)]. Interestingly, acute deletion of Zeb2 by Cre-vector electroporation (Fig. 5D) led to detectable levels of Sox6, suggesting that Sox6 was either induced or failed to be downregulated when Zeb2 was removed after birth.

These results indicate that Sox6 may be a direct Zeb2 target in neurogenic cells of the postnatal V-SVZ. Using ChIP in mouse embryonic stem cells (ESCs) subjected to neural differentiation (Stryjewska et al., 2017), we checked whether Zeb2 binding is
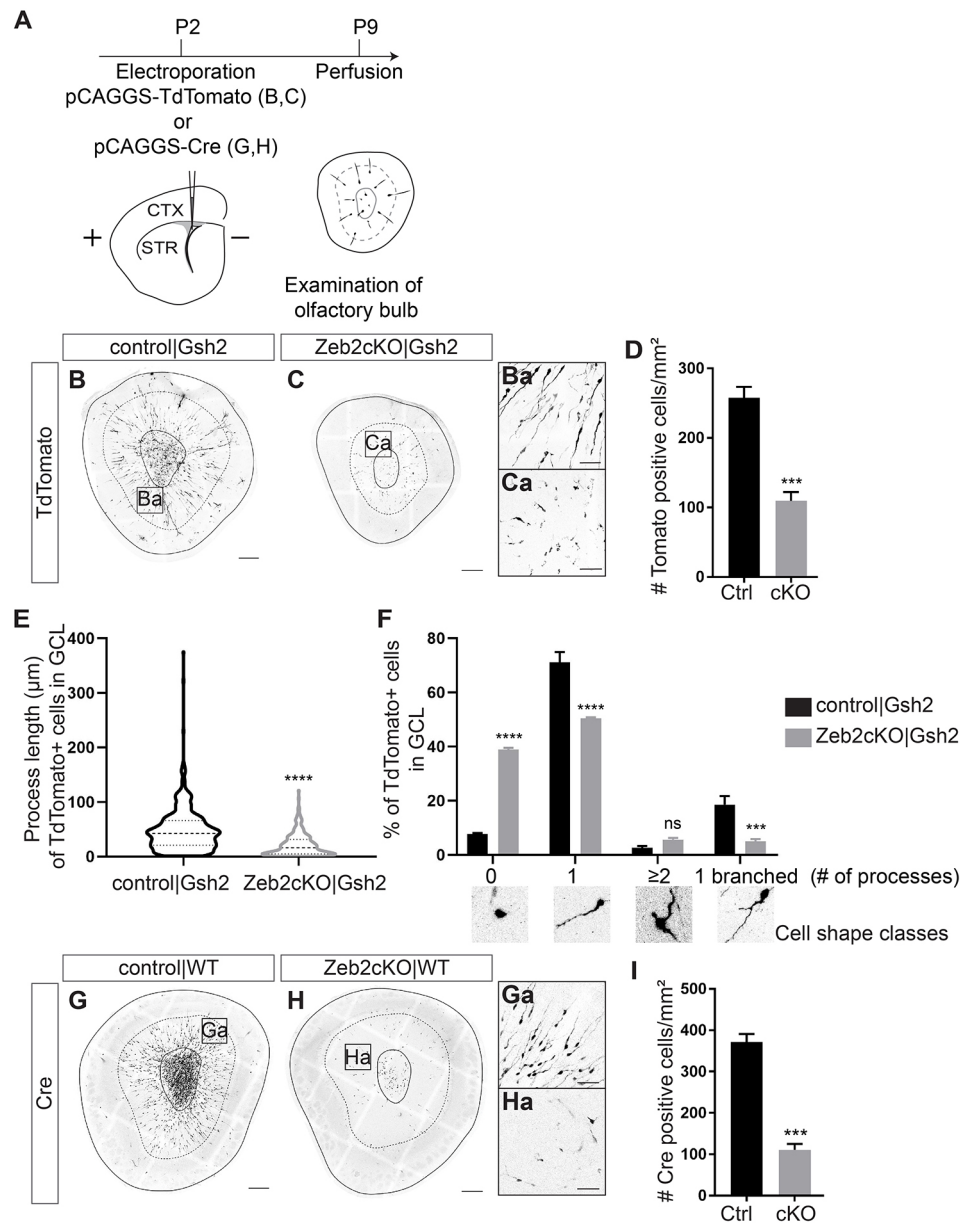
Fig. 2. Changes in embryonic and postnatal levels of Zeb2 in the V-SVZ have a major impact on OB interneuron numbers and maturation. (A) Overview of the electroporation experiment. TdTomato or Cre vectors were electroporated into V-SVZs at P2. Coronal OB sections were analyzed at P9. (B,C) Embryonic Gsh2-driven Zeb2 inactivation in the LGE led to a decrease of postnatally generated interneurons in mutants compared with controls. Magnifications (Ba,Ca) illustrate aberrant OB interneuron morphology in knockout mice. (D) Quantification of the number of TdTomato$^+$ cells/mm^2 in OBs at P9 (control, 257.7±15.7 versus cKO, 109.3± 12.9, two-tailed unpaired Student's t-test, ***P=0.001, n=4 for control and n=3 for cKO). (E,F) Morphological measurements of TdTomato$^+$ cells in the GCLs of the OB at P9. Violin plot showing process length (from soma to the end of the neurite) (E). Mean process length is represented by the dashed line and quartiles by dotted lines [mean in control, 48.39 μm (434 cells) vs cKO, 21.33 μm (242 cells), two-tailed unpaired Student's t-test, ****P<0.0001]. Leading process number sprouting (away from the RMS) from each soma and branching of the process (F). In the knockout, more interneurons without processes (7.742% in control versus 38.89% in cKO, ****P<0.0001), fewer interneurons with one process (71.08% in control versus 50.39% in cKO, ****P<0.0001) and fewer interneurons with a branched process (18.55% in control versus 5.06% in cKO, ***P<0.01) were observed. Representative images of each cell shape class are shown under the graph. The total amount of quantified cells is 1453 for control and 574 for cKO, each measured in three independent animals (two-way ANOVA). (G-H) Acute postnatal inactivation of Zeb2 in the V-SVZ led to a similar phenotype. Magnifications (Ga,Ha) show that postnatal loss of Zeb2 also results in aberrant OB interneuron morphology. (I) Quantification of the number of Cre-induced GFP$^+$ cells/mm^2 in OBs at P9 (control, 371.4±19.7 versus cKO, 110.8±14.2, two-tailed unpaired Student's t-test, ***P<0.001, n=3 for control and cKO). Lines in B,C,G,H indicate GCL borders. Data are mean±s.e.m. CTX, cortex; STR, striatum. ns, not significant. Scale bars: 200 μm (B,C,G,H); 50 μm (Ba,Ca,Ga,Ha).

enriched in the promoter-proximal regulatory regions of *Sox6*. In line with our previous results (Stryjewska et al., 2017), we found that both Zeb2 and Sox6 mRNA levels increased from day 4 of differentiation but Sox6 mRNA remained relatively low compared with Zeb2 mRNA (Fig. 5E). In day 6 and day 8 cells, we found significant enrichment of Zeb2 binding to its cognate

sites in the 4 kb region upstream of the *Sox6* transcription start site, suggesting that Zeb2 is a candidate direct repressor of *Sox6* (Fig. S8).

When translated to postnatal neurogenesis, these results suggest that overproduction of Sox6 in the wild-type V-SVZ may lead to decreased OB interneuron production, thereby recapitulating the
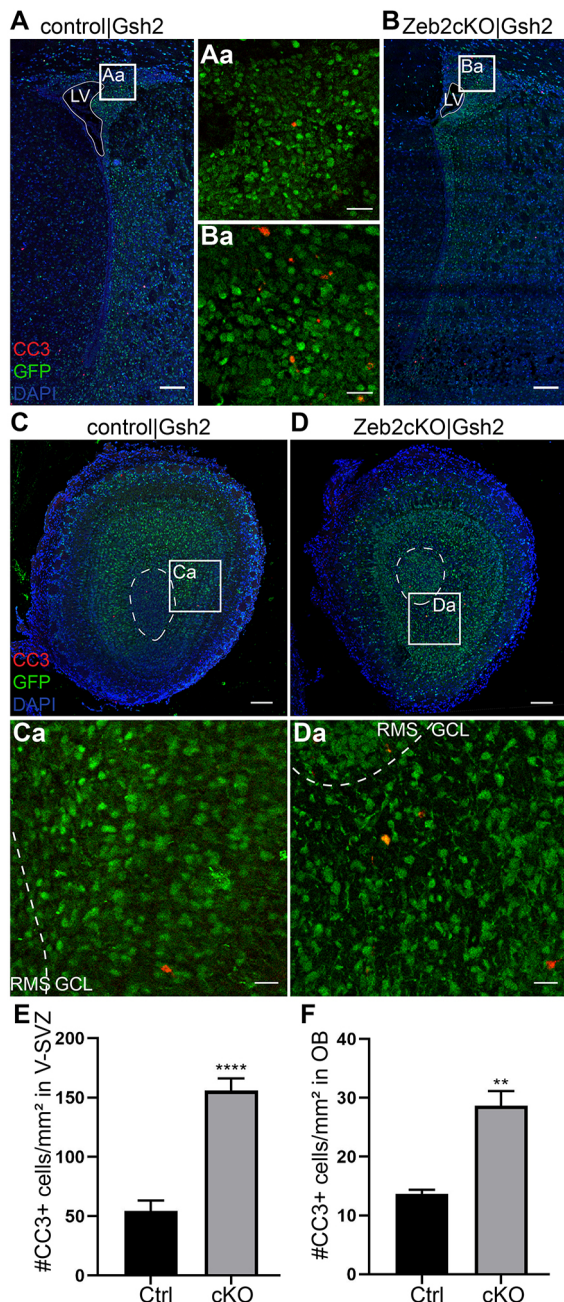
Fig. 3. Apoptosis is increased in the postnatal V-SVZ and OB in absence of Zeb2. (A-Ba,E). Analysis of apoptosis (cleaved caspase 3, CC3 immunostaining) on coronal sections at P5. The number of CC3$^+$ cells is significantly increased in the Zeb2cKO|Gsh2 V-SVZ (B,Ba) compared with the control (A,Aa; quantification in E: 55.4 cells/mm^2 in control versus 155.9 cells/mm^2 in cKO, two-tailed unpaired Student's t-test, ****$P<0.0001$, n=8). (C-Da,F) A similar increase is found in the Zeb2cKO|Gsh2 OB compared with the control (quantification in F: 13.6 cells/mm^2 in control versus 28.7 cells/mm^2 in cKO, two-tailed unpaired Student's t-test, **$P<0.01$, n=3). Dashed lines indicate the RMS border. Data are mean±s.e.m. GCL, granule cell layer; LV, lateral ventricle; RMS, rostral migratory stream. Scale bars: 100 µm (A,B,C,D); 20 µm (magnified boxes in Aa,Ba,Ca,Da).

Zeb2-cKO phenotype. To test this, we electroporated a (TdTomato and) Sox6-expression vector in the V-SVZ at P2, and quantified the TdTomato$^+$ cells in the OBs at P9 (Fig. 5F). A strong reduction in the number of TdTomato$^+$ cells was found compared with controls (Fig. 5G-I). Of note, we also found similarly aberrant and stunted

cellular morphology, comparable with the OB interneurons of *Zeb2*-cKO mice (Fig. 5Ga,Ha). Taken together, these results suggest that Sox6 probably acts downstream of Zeb2.

Different known Zeb2 protein-interacting domains support distinct functions in OB interneuron generation and maturation

To investigate the functions of various known Zeb2 domains in OB interneuron development, we carried out cDNA-based rescue experiments by electroporation (Fig. 6A). For this, we first used a full-length Zeb2 (Zeb2^{WT}, Fig. 6B) expression vector in the Zeb2cKO|Gsh2 V-SVZ at P2 (Fig. 6D). As a negative control, we used an NZF/CZF double zinc-finger mutant of Zeb2 (Zeb2^{ZnF}), which is incapable of binding to DNA (Remacle et al., 1999) (Fig. 6C). This Zeb2^{ZnF} mutant was not able to rescue defective OB interneuron output or interneuron morphology. In contrast, Zeb2^{WT} resulted in a 78% increase in neurons, which now, once again, reached the OB when compared with Zeb2^{ZnF} (Fig. 6C,D; quantification in G). Furthermore, most interneurons in this rescue presented with a longer radially pointing process, away from the RMS, with several of such cells showing branched processes (Fig. 6H,I).

In Zeb2^{SBD}, four crucial amino acids needed for Smad-binding are substituted, making this mutant protein incapable of binding to activated Smads (Conidi et al., 2013). Electroporation of Zeb2^{SBD} resulted in a significantly higher output to the OB (115% increase) and rescued the bipolar morphology, process length and branching of the cells (Fig. 6F; quantification in G-I). Interestingly, Zeb2^{NIM} [(a mutant that no longer binds to NuRD (Verstappen et al., 2008; Wu et al., 2016)] did not rescue OB interneuron numbers but enhanced the formation of cellular processes, and rescued their length and branching capacity, albeit to a lesser extent than Zeb2^{SBD} (Fig. 6E; quantification in G-I). Overproduction of Zeb2^{ZnF}, Zeb2^{WT} and Zeb2^{NIM} in control|Gsh2 mice resulted in similar cell outputs to the OB, whereas Zeb2^{SBD} caused a 35% increase in the number of neurons that arrived at the OB compared with Zeb2^{ZnF} (Fig. 6F, quantification in G).

Taken together, these results show that in the early postnatal V-SVZ, Zeb2 is essential for the production of sufficient numbers of OB interneurons and for the acquisition of their proper morphology. Furthermore, our experiments indicate that interaction of Zeb2 with receptor-activated Smads normally negatively regulates interneuron output, whereas interaction with NuRD is necessary for cell maturation but has no impact on cell number.

DISCUSSION

Zeb2 is implicated in many developmental processes, including exit from epiblast stem cell (-like) pluripotency in ESC cultures (Stryjewska et al., 2017) and in the development of the central and peripheral nervous systems (CNS and PNS) (for recent reviews, see Hegarty et al., 2015; Epifanova et al., 2019). Here, we show that Zeb2 determines the numeric output from the V-SVZ niche and is needed for the normal distribution and maturation of postnatally generated OB interneurons. Furthermore, Zeb2 binds to the *Sox6* promoter and is needed for proper *Sox6* expression control, thereby promoting the differentiation of V-SVZ-derived cells. In addition, Zeb2 removal also impacts on the proliferation and differentiation of non-targeted resident cells. Our results further indicate the novel finding that Zeb2 uses particular functional domains to perform distinct functions in OB interneuron development, as addressed by cDNA-based rescue experiments in the *Zeb2*-cKO V-SVZ.
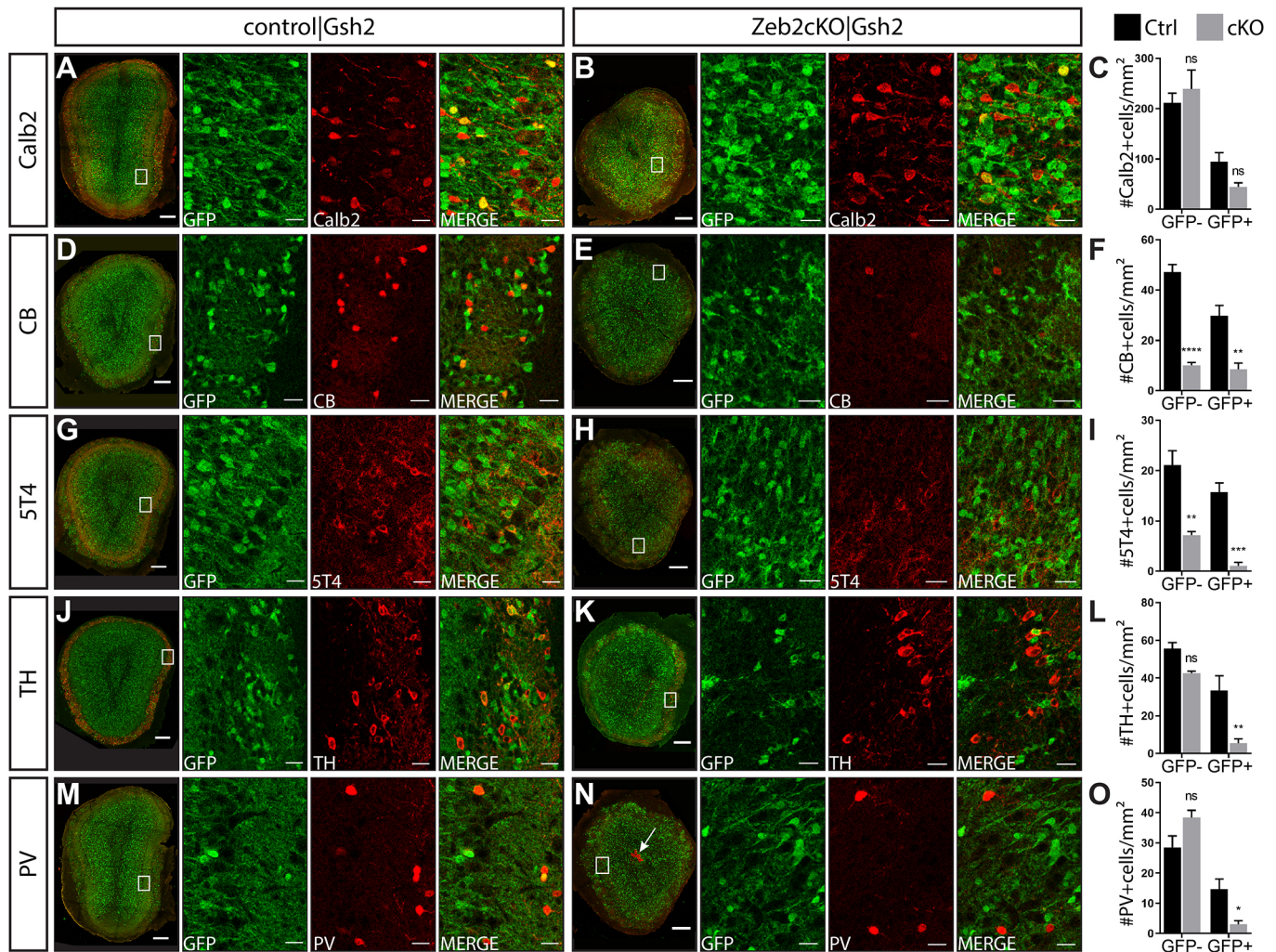
Fig. 4. Zeb2 steers the differentiation and distribution of distinct OB interneuron subtypes in a cell-autonomous and non-cell-autonomous manner. (A-O) Characterization of OB interneuron types at P18 in control|Gsh2 and Zeb2cKO|Gsh2 mice. Relative to OB size, the number of Calb2$^+$ cells did not change (A-C), whereas the numbers of CB$^+$ and 5T4$^+$ cells decreased in both the targeted (GFP$^+$) as well as the non-targeted (GFP$^-$) population in Zeb2cKO|Gsh2 mice compared with the control (D-I). A decrease in the TH$^+$ and PV$^+$ targeted population can also be observed in the Zeb2cKO|Gsh2 mice (J-O). For PV, a particular misplacement of non-targeted cells was found in the Zeb2cKO|Gsh2 RMS (N, arrow) (1% of PV$^+$ cells in control versus 43% in cKO, *$P<0.01$). All quantifications are listed as control|Gsh2 versus Zeb2cKO|Gsh2 in number of marker$^+$ cells/mm^2 (two-way ANOVA). Calb2: GFP$^-$: 221.6 versus 238.9, $P=0.68$, GFP$^+$: 94.71 versus 44.64, $P=0.30$; CB: GFP$^-$: 47.09 versus 10.06, ****$P<0.0001$, GFP$^+$: 29.68 versus 8.48, **$P<0.01$; 5T4: GFP$^-$: 21.09 versus 7.16, **$P<0.01$, GFP$^+$: 15.74 versus 1.08, ***$P<0.001$; TH: GFP$^-$: 55.64 versus 42.65, $P=0.13$, GFP$^+$: 33.43 versus 5.48, **$P<0.01$; PV: GFP$^-$: 28.53 versus 38.40, $P=0.08$, GFP$^+$: 14.65 versus 3.07, *$P<0.05$; $n=3$ for all groups. Data are mean±s.e.m. 5T4, oncofetal trophoblast glycoprotein; Calb2, calretinin; CB, calbindin; PV, parvalbumin; SST, somatostatin; TH, tyrosine hydroxylase. ns, not significant. Scale bars: 200 µm; 20 µm (higher magnification).

Zeb2 as a promoter of cell survival, fate specification, and cell differentiation and maturation

In the V-SVZ niche and its progeny, Zeb2 mRNA/protein is present at different temporal levels, being high in V-SVZ C and A cells, decreasing in migrating RMS neuroblasts and becoming more prominent again in cells that progress through differentiation in olfactory periglomerular and granular interneurons. The increased expression upon differentiation in the OB is similar to the one described for other tissues and cells, such as the embryonic cerebral cortex, in which Zeb2 is exclusively present in postmitotic cells (Seuntjens et al., 2009), the embryonic ventral telencephalon, in which it becomes prominent in migrating interneurons (Batista-Brito et al., 2008a; McKinsey et al., 2013; van den Berghe et al., 2013), as well as in immune cell maturation (Omilusik et al., 2015; van Helden et al., 2015; Scott et al., 2016), and in human and mouse neural-induced ESCs (Chng et al., 2010; Stryjewska et al., 2017).

Here, the pattern suggests Zeb2 plays a role in the V-SVZ niche itself, in particular in the C cells and the neuroblasts, as well as in OB interneurons.

These results, together with the aberrant morphology and reduced numbers of Zeb2-deficient OB interneurons, possibly reflect maturation defects. Similarly, its absence in GABAergic interneurons leads to the deregulation of genes involved in processes such as synaptogenesis and synaptic plasticity (van den Berghe et al., 2013), and the absence of Zeb2 also affects midbrain dopaminergic neuron differentiation (Hegarty et al., 2017). Another striking phenotype of Zeb2cKO|Gsh2 mice observed in our study was the failure to populate the OB with neuroblasts in early postnatal life and the reduced output of migrating Dcx$^+$ neuroblasts. We propose that this shortage of OB interneurons in the *Zeb2*-cKO underlies the aberrant OB morphology. Similar disorganization of OB interneurons was observed in Dlx5/6-driven *Sp8* and *Sp9*-cKO
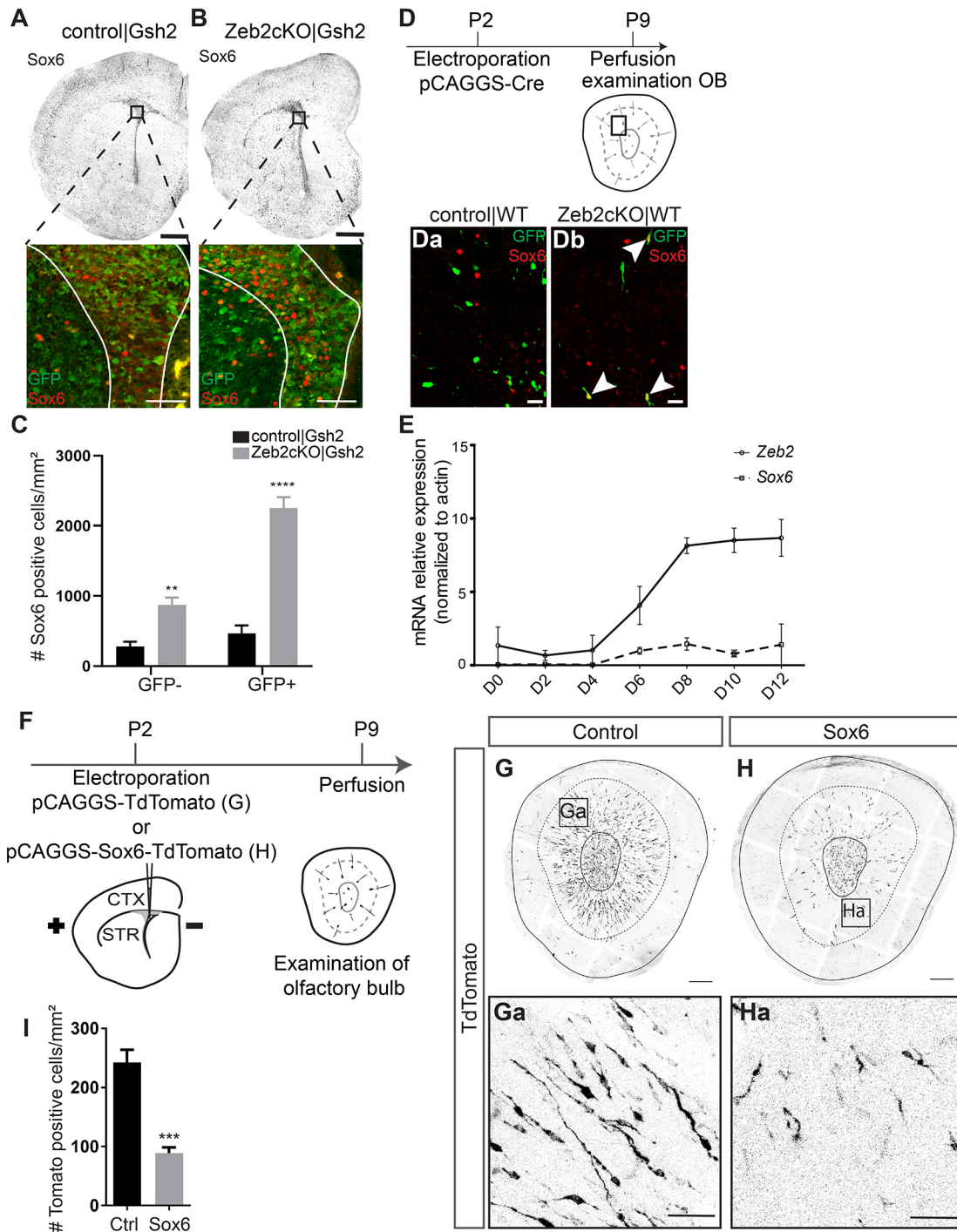
Fig. 5. *Sox6* is strongly upregulated in the Zeb2cKO|Gsh2 V-SVZ and postnatal overproduction of Sox6 in the V-SVZ mimics loss of Zeb2. (A,B) Staining for Sox6 at P5 in control and mutant V-SVZ. A representative image for GFP and Sox6 is shown in which the increase of Sox6 in both GFP$^+$ and GFP$^-$ cells is illustrated. (C) Number of Sox6$^+$ cells in the control|Gsh2 and Zeb2cKO|Gsh2 V-SVZ (for GFP$^-$: 281.3 in control versus 873.2 cells/mm^2 in cKO, **P<0.01; for GFP$^+$: 462.9 in control versus 2254 cells/mm^2 in cKO, ****P<0.0001, two-way ANOVA, n=5). (D-Db) Coronal section through the P9 OB after electroporation of a pCAGGS-Cre construct in the V-SVZ (floxed Zeb2) at P2. Boxed area in the OB indicates the magnified region, showing a clearly elevated level of Sox6 in targeted cells upon acute *Zeb2* inactivation (arrowheads). (E) Normalized expression of *Zeb2* and *Sox6* after ChIP in mouse ESCs subjected to neural differentiation. Zeb2 and Sox6 mRNA levels started increasing from day 4 (D4) of differentiation onwards. (F) TdTomato- or Sox6-TdTomato-encoding vectors were electroporated into the wild-type V-SVZ at P2. Coronal OB sections were analyzed at P9. (G-H) Overproduction of Sox6 in the normal V-SVZ led to a significant decrease in the number of neuroblasts that arrived in the OB compared with the control. Magnifications (Ga,Ha) show that cells that overproduced Sox6 have a smaller cell body and thinner processes, and have a defect in laminar organization. (I) Number of TdTomato$^+$ cells/mm^2 in the OB at P9 (242.7±21.2 cells/mm^2 in control versus 89.0±9.7 cells/mm^2 in excess Sox6, two-tailed unpaired Student's *t*-test, ***P<0.001, n=5 for control and n=9 for excess Sox6). Data are mean±s.e.m. CTX, cortex; STR, striatum. Scale bars: 200 µm (20 µm in magnifications) (A,B); 20 µm (Da,Db); 200 µm (G,H); 20 µm (Ga,Ha).
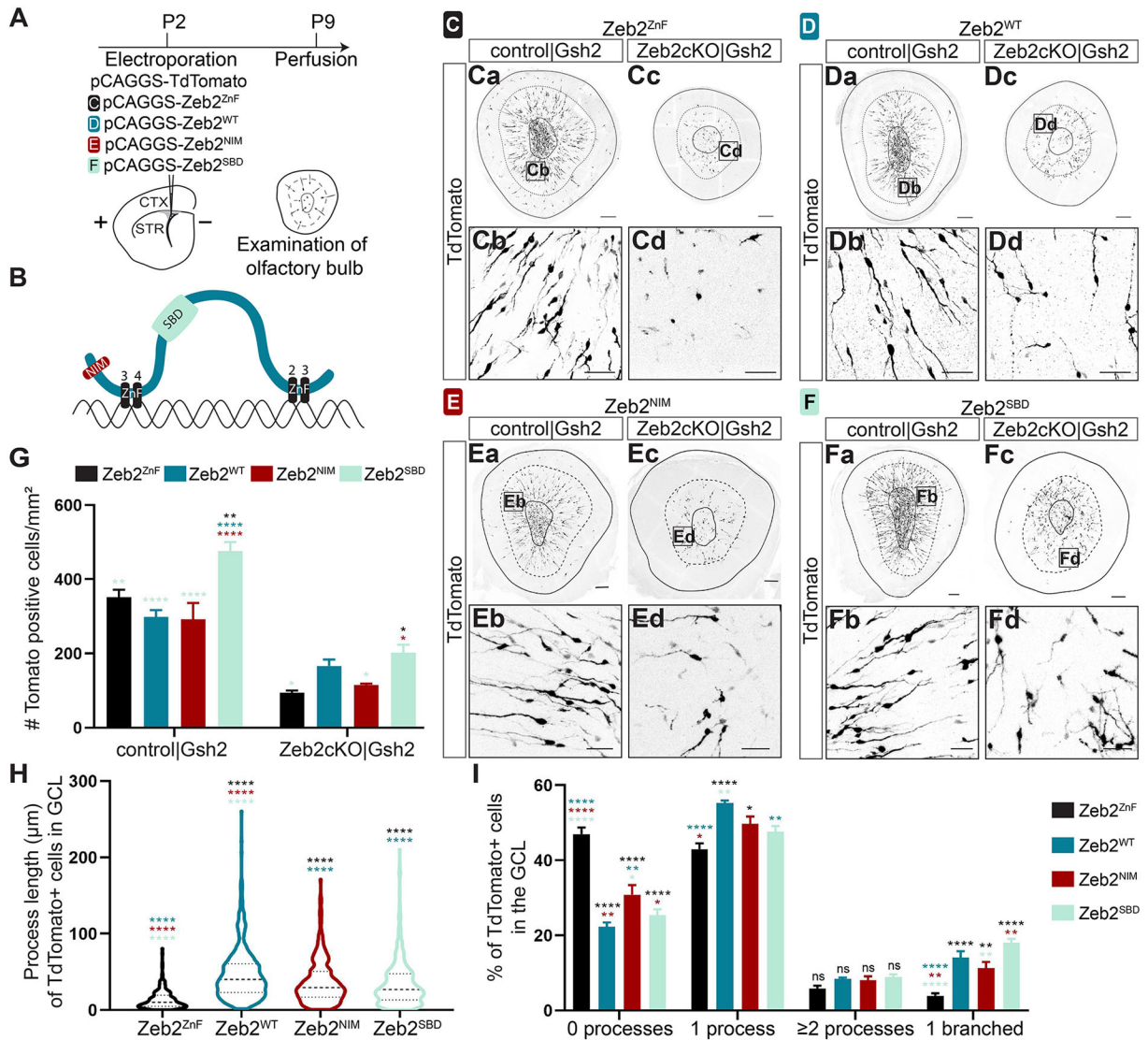
DEVELOPMENT

8

Fig. 6. Zeb2 domains contribute differently to neuroblast generation and maturation. (A) Schematic representation of electroporation of TdTomato- together with Zeb2^{WT}-, Zeb2^{ZnF}-, Zeb2^{SBD}- or Zeb2^{NIM}-encoding vectors at P2 in V-SVZ. Coronal OB sections were analyzed at P9. (B) Schematic representation of Zeb2, bound to DNA via specific zinc fingers in NZF and CZF. The NIM is located at the N-terminus and the SBD is present between the two ZnF domains. (C-F) Postnatal reintroduction of Zeb2 in control and Zeb2cKO|Gsh2 V-SVZ. Zeb2^{ZnF} mutant phenocopied the Zeb-cKO. Reintroduction of wild-type Zeb2 (Zeb2^{WT}), Zeb2^{SBD} or Zeb2^{NIM} mutant protein affected the number of cells reaching the OB, as well as their morphology. (G) Quantification of the relative amount of OB interneurons (numbers of TdTomato$^+$ cells/mm^2, two-way ANOVA) at P9. Only reintroduction of Zeb2^{WT} or Zeb2^{SBD} resulted in an increase in the number of OB interneurons compared with Zeb2^{ZnF} (Zeb2^{WT}: $P=0.15$, Zeb2^{SBD}: *$P=0.01$). Overexpression of Zeb2^{SBD} in control|Gsh2 mice significantly raised the number of neurons that migrate to the OB (versus Zeb2^{ZnF} **$P<0.01$, versus Zeb2^{WT} ****$P<0.0001$, versus Zeb2^{NIM} ****$P<0.0001$). Zeb2^{ZnF}: control|Gsh2, 351.5 cells/mm^2 (n=4); Zeb2cKO|Gsh2, 93.87 cells/mm^2 (n=3); Zeb2^{WT}: control|Gsh2, 298.3 cells/mm^2 (n=4); Zeb2cKO|Gsh2, 166.7 cells/mm^2 (n=3); Zeb2^{NIM}: control|Gsh2, 292.7 cells/mm^2 (n=3); Zeb2cKO|Gsh2, 115.2 cells/mm^2 (n=4); Zeb2^{SBD}: control|Gsh2, 476.3 cells/mm^2 (n=4); Zeb2cKO|Gsh2, 202.1 cells/mm^2 (n=3). (H,I) Morphological measurements of TdTomato$^+$ cells in the GCLs of the OB at P9. Violin plot showing process length (from soma to end of the neurite) measured in µm (H). Zeb2^{SBD}, as well as Zeb2^{NIM}, partially rescue, whereas Zeb2^{WT} rescued the neurite length significantly more. Mean process length is represented by the dashed line and quartiles by dotted lines. Mean process length for all constructs: Zeb2^{ZnF}, 13.64 µm (242 cells); Zeb2^{WT}, 48.05 µm (389 cells); Zeb2^{NIM}, 36.85 µm (312 cells); Zeb2^{SBD}, 34.87 µm (532 cells). All constructs differ significantly (two-way ANOVA, $P<0.0001$) from one another except Zeb2^{NIM} and Zeb2^{SBD}, which showed similar process lengths. Leading process number sprouting (away from the RMS) from each soma and branching of the process (I). All rescue constructs showed less cells without sprouting and more cells with one (branched) process compared with the Zeb2^{ZnF} control. The Zeb2^{NIM} construct was less potent in rescuing the number of cells without processes compared with the Zeb2^{WT} (**$P<0.01$) and Zeb2^{SBD} (*$P<0.05$), and had fewer branched processes compared with the Zeb2^{SBD} ($P<0.01$) but not Zeb2^{WT}. The total amount of cells quantified are 727, 1327, 845 and 1598 cells for ZnF, WT, NIM and SBD constructs, respectively; all from at least three animals (two-way ANOVA). Data are mean±s.e.m. CTX, cortex; NIM, NuRD interaction motif; OB, olfactory bulb; SBD, Smad binding domain; STR, striatum; SVZ, subventricular zone; ZnF, Zinc Finger. Scale bars: 200 µm (Ca,Cc,Da,Dc,Ea,Ec,Fa,Fc); 50 µm (Cb,Cd,Db,Dd, Eb,Ed,Fb,Fd).

mice (Waclaw et al., 2006; Li et al., 2018). In *Sp8*-cKO animals, however, apoptosis in the V-SVZ, and neuroblast migration and molecular specification defects, were exclusively due to defective cell-autonomous actions of Sp8 (Li et al., 2018).

Functionally integrated mature interneurons in the GCL of the OB display extensively branched dendritic arbors, and those in the glomerular layer usually have two branched processes (Price and Powell, 1970; Merkle et al., 2014; Figueres-Oñate and López-

Mascaraque, 2016). Although our electroporated cells were 1 week old at most (and hence not fully mature), the processes of the interneurons lacking Zeb2 were absent or shorter, and 73% less branched compared with controls. A cell-autonomous role for Zeb2 operates in the determination of axon length of hippocampal and neocortical cells *in vitro*, as well as in axon branching in the cortex in which neurons lacking Zeb2 have shorter processes and show less branching, respectively (Srivatsa et al., 2015).

To limit the amount of OB interneurons, about half of the progenitors and young neuroblasts undergo programmed cell death during adult neurogenesis (Winner et al., 2002). Apoptosis is typically more frequent upon the integration of new neurons into an existing network, such as that of the OB, and failure to receive sensory input triggers cell loss (Corotto et al., 1994; Petreanu and Alvarez-Buylla, 2002; Rochefort et al., 2002). Our results indicate that Zeb2 is required for cell survival in both OB interneuron progenitors in the V-SVZ and in the differentiating interneurons themselves. It remains unclear whether apoptosis is a direct consequence of Zeb2 loss in OB interneurons, or whether the truncated morphology of *Zeb2*-KO OB interneurons impairs their functional integration and indirectly triggers apoptosis. Loss of Zeb2 itself has also been linked to apoptosis in cancer cell lines, as well as during retinal development, in which the deletion of Zeb2 induces DNA damage-induced apoptosis (Sayan et al., 2009; Qi et al., 2012; Wei et al., 2019).

Zeb2 enables OB interneuron production and maturation via downregulation of *Sox6*

Sox6 is upregulated in the *Zeb2*-cKO V-SVZ, suggesting that postnatal niche progenitors need to repress *Sox6* to allow for the production of sufficient numbers of correctly specified future OB interneurons. Sox6 co-determines cell diversification in the telencephalon, substantia nigra and ventral tegmental area during development (Azim et al., 2009; Batista-Brito et al., 2009; Panman et al., 2014). In early postmitotic neurons destined for the cortex [medial ganglionic eminence- (MGE) born], Sox6 acts downstream of Lhx6 and Nkx2-1, regulating tangential migration and distribution, and eventually the differentiation and maturation of cortical PV and somatostatin interneurons (Azim et al., 2009; Batista-Brito et al., 2009). Conversely, excessive Sox6 in the *Zeb2*-cKO V-SVZ might drive the aberrant appearance of PV$^+$ neuroblast-like cells within the RMS. A similar upregulation of *Sox6* occurs in *Zeb2*-cKO cortical interneurons, also resulting in defects in interneuron specification, guided migration and maturation (McKinsey et al., 2013; van den Berghe et al., 2013).

Our results clearly show that Sox6 overproduction leads to a decreased neuronal output and aberrant cell shape in the OB, similar to the *Zeb2*-KO or Zeb2^{ZnF} rescue. *Sox6* transcriptional regulation by Zeb2 is possibly direct, as suggested by ChIP-qPCR. Impaired DNA binding by the Zeb2^{ZnF} mutant could then also impact on the transcriptional repression of *Sox6*, resulting in similar outcomes.

The non-cell-autonomous mode of action of Zeb2

Removing Zeb2 from a large proportion of V-SVZ cells consistently affects non-targeted cells. Within the V-SVZ niche, these cells show a reduction in proliferation, as well as an elevation in *Sox6* expression. From our apoptosis study, non-cell-autonomous or indirect effects cannot be deduced in a reliable way because of the low number of CC3$^+$ cells. Nevertheless, in the mutant OB, the numbers of non-targeted 5T4$^+$, CB$^+$ and PV$^+$ cells are significantly reduced, similar to targeted cells. Non-cell-autonomous actions have been documented in the hippocampus anlage, in which *Zeb2* deletion impacts on proliferation and apoptosis via Wnt signaling. Cell-autonomous versus non-cell-autonomous effects were not further discriminated;

however, Sfrp1 (a Wnt antagonist) was upregulated in the absence of Zeb2, with the most prominent effects impacting postmitotic cells (Miquelajauregui et al., 2007). In the developing neocortex, an unprecedented but clear non-cell-autonomous role for Zeb2 has been documented in the timing of neurogenesis and gliogenesis. Via the neurotrophin Ntf3, Zeb2 regulates feedback signaling from postmitotic neurons to progenitors, coordinating the timing of the progenitor cell fate switch (Seuntjens et al., 2009; Parthasarathy et al., 2014). The nature of the non-cell-autonomous actions of Zeb2 in the postnatal V-SVZ remains to be studied in detail.

Zeb2 protein domains control distinct aspects of OB interneuron development

Although various roles and action mechanisms downstream of Zeb2 have been documented in many tissues during development, the precise roles that are served by the direct interaction of Zeb2 with one or more known co-factors have not always been addressed (Van Grunsven et al., 2003; van Grunsven et al., 2007; Verstappen et al., 2008; Wu et al., 2016). Our study is one of the first to show that Zeb2^{WT} protein, and Zeb2^{NIM} and Zeb2^{SBD} mutants bear different rescue capacities in both quantitative and qualitative terms. The most likely explanation could be the change in balance between repressor activity of Zeb2 on a set of target genes versus activator activity on another set of genes (reviewed by Conidi et al., 2011). This dual role has been observed in neuroectoderm differentiation of human ESCs (Chng et al., 2010), embryonic hematopoiesis (Goossens et al., 2011), CNS myelinogenesis (Weng et al., 2012) and adult PNS (Schwann cell mediated) myelination (Quintes et al., 2016; Wu et al., 2016). In these myelinogenesis and (re)myelination studies, Zeb2 generates anti-BMP-Smad and anti-Wnt-β-catenin activities where needed, as well as (in adult Schwann cells) additional anti-Notch and anti-Sox2 activities. Zeb2 is thus clearly a cell differentiation and process regulatory protein that fulfills a role as a context-dependent integrator of multiple signaling pathways.

Introducing the Zeb2^{SBD} mutant into the Zeb2cKO|Gsh2 V-SVZ leads to increased numbers of OB interneurons, indicating that Zeb2-Smad cooperation is crucial for tightly regulating the output capacity of niche progenitors. Intriguingly, a similar stronger rescue of neural differentiation is found when a neural induction protocol is applied to mouse *Zeb2*-KO ESCs overexpressing Zeb2^{SBD} compared with overexpressing Zeb2^{WT} (Stryjewska, 2016). This might point towards a more general phenomenon in the context of (neural) stem cells, in which Zeb2-Smad interaction inhibits neural differentiation and cell survival. The core motif essential for Zeb2-Smad interaction is a QxVx repeat in a 14 amino acid segment of the initially defined 51 amino acid SBD (Verschueren et al., 1999; Conidi et al., 2013). Mutation of the motif into AxAx made Zeb2 incapable of rescuing the migration defect of *Zeb2*-KO cortical interneurons and perturbed the dose-dependent downregulation of TGFβ/BMP-Smad signaling (Conidi et al., 2013). Therefore, BMP-promoted cell survival might be affected (Grotewold and Rüther, 2002; Sharov et al., 2003). In addition, Smad4, the common-mediator Smad (ten Dijke and Heldin, 2006), is a key regulator of the directional progression of postnatal V-SVZ NSCs towards the neuronal lineage (Colak et al., 2008; Kawaguchi-Niida et al., 2017). Conditional *Smad4* deletion in V-SVZ progenitors results in an increase of NSC-like properties and differentiation defects (Kawaguchi-Niida et al., 2017). We propose that the introduction of Zeb2^{SBD} in a *Zeb2*-KO background renders the cells incompetent to correctly regulate Smad family signaling, potentially leaving the cells for a longer period in the proliferative phase preceding their differentiation into OB interneurons and preventing apoptosis.

10

In contrast to the obtained rescue in the Zeb2cKO|Gsh2 V-SVZ by the mutant Zeb2^{SBD}, the introduction of the Zeb2^{NIM} mutant leads to a rescue of OB interneuron morphology but fails to significantly increase cell numbers. Zeb2^{NIM} protein can no longer recruit NuRD (including the subunits HDAC1/2), which results in reduced Zeb2-NuRD-mediated transcriptional repression (Verstappen et al., 2008; Wu et al., 2016). This intermediate rescue may be reminiscent of the milder forms of MOWS caused by mutations in the NIM of Zeb2 (Yoneda et al., 2002; Zweier et al., 2006; Verstappen et al., 2008).

Taken together, our results show that Zeb2, through two of its known domains, is crucial for generating sufficient numbers of OB interneurons and ensuring their proper maturation. Our study shows for the first time how the respective Zeb2 SBD and NIM domains contribute to fulfilling these roles. However, which direct target genes, as well as intact Zeb2 domain-dependent genes are affected by the mutation of these respective domains, and whether these domains, besides co-determining cell-autonomous actions, also contribute to non-cell-autonomous actions of Zeb2, remains to be investigated.

MATERIALS AND METHODS
Animals
All mice were maintained in the CD-1/Swiss background and kept at KU Leuven according to local ethical committee approval that follows current Belgian and EU regulations. Mice carrying a floxed *Zeb2* allele (the largest exon 7, equivalent to exon 8 in human) (named as *Sip1$^{fl/fl}$* by Higashi et al., 2002) were crossed with Gsh2-Cre (Kessaris et al., 2006; Fogarty et al., 2007), Dlx5/6-Cre-IRES-GFP (Stenman et al., 2003) and *RCE$^{fl/fl}$*-reporter mice (*R26R$^{CAG-loxP-stop-loxP-eFP}$*; Sousa et al., 2009). We refer to the respective genotypes of the mice as indicated in Table 1 (using the Gsh2-Cre approach as an example; see also Seuntjens et al., 2009); a similar convention is used for the Dlx5/6-Cre approach.

DNA constructs
Expression vectors used in electroporation experiments were based on pCIG (a pCAGGS-IRES-eGFP plasmid; Megason and McMahon, 2002) obtained from P. Vanderhaeghen (Universite Libré de Bruxelles, Brussels, Belgium) wherein eGFP was replaced by TdTomato. For the deletion of *Zeb2* from the postnatal V-SVZ in *Zeb2$^{fl/ko}$* mice, a pCAGGS-Cre vector was used (H. Cremer, Institut de Biologie du Développement de Marseille, Marseille, France). Myc-tagged Zeb2^{WT} (Verschueren et al., 1999) and the mutants Zeb2^{ZnF} (Remacle et al., 1999), Zeb2^{NIM} (Wu et al., 2016) and Zeb2^{SBD} (Conidi et al., 2013) have been described previously. The Sox6 vector was generated by insertion of the blunted Sox6 cDNA-coding region [pCMV-3FLAG-Sox6 plasmid (V. Lefebvre, Children's Hospital of Philadelphia, Philadelphia, PA, USA) between NheI and XhoI] into the SmaI-cut pCAGGS-TdTomato vector, in between the pCAGGS promoter and IRES sequences.

Postnatal electroporation
P2 pups were anesthetized by hypothermia and placed under cold light to facilitate visualization of the brain lateral ventricles by transillumination. A 1.5 µl volume of plasmid mix (3 µg/µl DNA, 3% Fast Green) was injected into the left ventricular cavity. Electroconductive gel (Signagel, Parker Laboratories) was placed on both electrode paddles to avoid damaging the pups and achieve successful current flow. Five 100 V electric pulses were

Table 1. Terminology of mouse genotypes (using the Gsh2-Cre-based approach as an example)

Genotype	Terminology
Gsh2^{Cre+}; Zeb2$^{fl/wt}$	Control|Gsh2
Gsh2^{Cre+}; Zeb2$^{fl/ko}$	Zeb2cKO|Gsh2
Gsh2^{Cre-}; Zeb2$^{fl/wt}$	Control|WT
Gsh2^{Cre-}; Zeb2$^{fl/ko}$	Zeb2cKO|WT

applied (50 ms each, with 950 ms intervals), with the positive electrode positioned in the dorso-lateral region for directing DNA to the V-SVZ. After the pulses, the pups were placed on a thermal plate to recover, after which they were returned to their mother.

Tissue processing
Embryonic brains were isolated and washed in ice-cold PBS before overnight fixation in 4% paraformaldehyde in PBS. For all postnatal ages, mice were deeply anesthetized with an intraperitoneal injection of pentobarbital before intracardiac perfusion with ice-cold saline followed by fixative. Afterwards, brains were removed and fixed overnight at 4°C, and then washed in PBS. For electroporation experiments, 100 µm vibratome sections were used. For marker analysis, overnight fixation was followed by progressive dehydration and paraffin embedding, after which 6 µm coronal sections were cut.

Immunohistochemistry
Paraffin-embedded brain sections were processed using an automated platform with a DABMAP detection kit (DAB stainings; Fig. 1F-I) or without a detection kit (fluorescent stainings) (Ventana Discovery, Roche). Primary antibodies used were diluted in antibody diluent (Roche) or Pierce Immunostain Enhancer (Invitrogen) to enhance fluorescence signal at the final concentrations as follows: rabbit anti-Sip1 (anti-Zeb2, custom made, 1:1200; Seuntjens et al., 2009), chicken anti-GFP (Abcam, ab13870, 1:600), mouse anti-GFAP-Cy3 (Sigma-Aldrich, C9205, 1:300), goat anti-EGFR-biotin (R&D systems, BAF1280, 1:60), guinea pig anti-Dcx (Millipore, AB2253, 1:300), rabbit anti-Ki67 (Novocastra, NCL-Ki67p, 1:300), rabbit anti-phospho-Histone H3 (Ser10) (Millipore, 06-570, 1:300), rabbit anti-cleaved caspase-3 (Asp175) (Cell Signaling Technology, 9661S, 1:900), rabbit anti-calretinin (Abcam, ab92341, 1:150), rabbit anti-CB (Chemicon International, AB1178, 1:300), sheep anti-5T4 (Thermo Fisher Scientific, PA5-47690, 1:120), rabbit anti-TH (Millipore, AB152, 1:300), rabbit anti-PV (Swant, PV27, 1:3000), rabbit anti-Sox6 (Abcam, ab30455, 1:300) and mouse anti-reelin (a gift from Dr A. Goffinet, University of Leuven, Brussels, Belgium, 1:300). Secondary antibodies used were: donkey anti-chicken Alexa 488, donkey anti-goat Cy3, donkey anti-rat Cy3, donkey anti-rabbit Alexa 555, donkey anti-rabbit Alexa 488, donkey anti-guinea pig Cy3, donkey anti-sheep Cy3, streptavidin Alexa 594, donkey anti-chicken biotin-SP and donkey anti-rabbit biotin-SP (all 1:600, Jackson ImmunoResearch); and donkey anti-mouse Alexa 555, donkey anti-rat Alexa 594 and donkey anti-rabbit 594 (all 1:300, Life Technologies). Sections were imaged using a Leica DMR microscope connected to a Spot camera (Visitron Systems) or a confocal microscope (Leica SP8 X).

Vibratome brain slices were pre-incubated for 1 h in PBS containing 0.3% Triton X-100 (PBST) and 10% normal donkey serum. Primary antibodies (rabbit anti-RFP, Rockland, 600-401-379, 1:10,000; and chicken anti-GFP, Abcam, ab13870, 1:1000) were added overnight at 4°C. Following repeated washing in PBST, secondary antibodies (donkey anti-rabbit Alexa 594, Life Technologies, 1:200; and donkey anti-chicken Alexa 488, Jackson ImmunoResearch, 1:500) were applied for 2 h at room temperature. Slices were washed in PBST and mounted in Mowiol. Images were taken with a confocal microscope (Leica SP8 X).

Image analysis
The number of GFP$^+$;Dcx$^+$ cells or the marker-driven mean fluorescence intensity (MFI) was quantified using ImageJ (Rueden et al., 2017). Dcx/GFP overlap was measured using ColocalizerPro software. At least three animals were used for each genotype. Results are represented as mean±s.e.m. Statistical significance was determined using Student's *t*-test (unpaired, two-tailed). The total amount of RFP$^+$, GFP$^+$ or OB interneuron marker$^+$ cells was quantified using the cell counter plug-in in Fiji (Schindelin et al., 2012). For electroporation experiments, animals with fewer than 40 electroporated cells in the V-SVZ on one section were excluded from analysis and all constructs had a similar electroporation efficiency. Process length was also measured in Fiji. At least three animals were used for each genotype and results are represented as mean±s.e.m. Statistical significance was determined using Student's *t*-test (unpaired, two-tailed) or, for multiple comparisons, using two-way ANOVA followed by Tukey's multiple comparisons test.

FACS of V-SVZ cells

V-SVZ tissue of Zeb2cKO|Gsh2 and control|Gsh2 brains was isolated in ice-cold HEPES-buffered Leibovitz's L15 medium (Invitrogen) and cut into small pieces. Cells were dissociated by Papain solution (150 ml per brain at 12 units/ml; Sigma-Aldrich) supplemented with DNase-I (30 units/ml; Roche) for 30 min at 37°C followed by mechanical dispersion, washed twice with Dulbecco's PBS (Lonza) and passed over a 70 mm cell strainer (BD Falcon). Highly fluorescent cells were sorted using an Aria I cell sorter (BD Biosciences) for RNA-seq or a SH800S cell sorter (Sony) for qPCR.

qPCR

qPCR was performed on the P5 V-SVZ of five Zeb2cKO|Gsh2 and five control mice. GFP$^+$ and GFP$^-$ cells were sorted in PBS and then lysed overnight in lysis buffer (37.9 mM Tris HCl, 75 mM EDTA, 75.8 mM NaCl, 0.75% SDS) with proteinase K (1 mg/ml, Invitrogen). DNA was isolated and qPCR was carried out in duplicate on a Bio-Rad CFX96 thermocycler using SYBR Green PCR Master Mix (Sso Advanced Universal SYBR Green Supermix, Bio-Rad).

RNA-seq and data analysis

RNA-seq was performed on the P2 V-SVZ of five Zeb2cKO|Gsh2 and six control mice. Sorted cells were immediately lysed in TRIzol LS (Invitrogen). RNA was extracted using an RNeasy Micro Kit (Qiagen). The RNA-seq library was prepared for analysis according to Illumina TruSeq protocols (www.illumina.com). Briefly, poly(A)-RNA was copied into cDNA, end repaired, (A) tailed, ligated with adaptors and enriched by PCR. RNA-seq library stocks were pooled and sequenced for 36 bp using the HiSeq-2000 sequencer. Low-quality single-end reads were first removed using fastq_quality_filter (FASTX-Toolkit) and the high-standard quality of all data was confirmed with FastQC. Reads were then mapped to the mouse genome GRCm38 using TopHat2 (v2.0.13). A count table for Ensembl-annotated genes was generated with featureCounts (v1.4.6). To assess differentially expressed genes, DESeq2 was applied using a pairwise contrast matrix (e.g. control|Gsh2 versus Zeb2cKO|Gsh2). For clustering, the samples were first transformed using the 'varianceStabilizingTransformation' in DESeq2, subsequently scaled and centered, and then separated based on Euclidean distance and complete linkage. PCA was applied to reduce dimensionality and visualize the samples in a two-dimensional space. Read coverage was visualized using the Integrative Genomics Viewer (Broad Institute). The RNA-seq data have been deposited with GEO under accession number GSE103003.

RT-qPCR

RNA was obtained from FAC-sorted P2 V-SVZ cells and cDNA was made using the SuperScript III First-Strand Synthesis System (Invitrogen). qPCR was performed on a LightCycler 480 (Roche) using SYBR Green PCR Master Mix (Roche).

Chromatin immunoprecipitation (ChIP)

Zeb2 ChIP was performed as described previously (Wu et al., 2016). Briefly, nuclei were isolated from 10^8 formaldehyde-fixed cells and isolated nuclear lysates were submitted to sonication (BioRuptor Sonicator, 30 s on, 15 s off, for 10 min altogether at high amplitude). Centrifuge-cleared sonicated material was then incubated in 1× ChIP buffer (10×: 0.2 M HEPES, 0.2 M NaCl, 0.02 M EDTA). A 50 μl volume of material was stored at −80°C to be used as input control and the rest was incubated with 7.5 μg of anti-Zeb2 (Santa Cruz Biotechnology, H-260, 1:75) for 16 h at 4°C. ChIP material was then incubated with 50 μl of Protein-A/G plus agarose beads (Santa Cruz Biotechnology, SC-2003) and rotated for 1 h at 4°C. DNA-protein complexes were then eluted from the beads with elution buffer [10 mM Tris-HCl (pH 8.0), 1% (w/v) SDS] at 65°C for 15–20 min, with gentle shaking. Samples were then incubated for 16 h with 50 μl of 5 M NaCl for reverse crosslinking, followed by digestion with 200 μg Proteinase K and then with 200 μg of RNaseA. DNA was precipitated and purified using a QIAquick PCR Purification Kit (Qiagen) and then stored at −20°C until needed for qPCR. The primers for qPCR are listed in Table S1.

References

Altman, J. (2011). The discovery of adult mammalian neurogenesis. In *Neurogenesis in the Adult Brain I* (ed. T. Seki and J. M. Parent), pp. 3-46. Dordrecht: Springer. doi:10.1007/978-4-431-53933-9_1

Alvarez-Buylla, A. and García-Verdugo, J. M. (2002). Neurogenesis in adult subventricular zone. *J. Neurosci.* **22**, 629-634. doi:10.1523/JNEUROSCI.22-03-00629.2002

Azim, E., Jabaudon, D., Fame, R. M. and Macklis, J. D. (2009). SOX6 controls dorsal progenitor identity and interneuron diversity during neocortical development. *Nat. Neurosci.* **12**, 1238-1247. doi:10.1038/nn.2387

Batista-Brito, R., MacHold, R., Klein, C. and Fishell, G. (2008a). Gene expression in cortical interneuron precursors is prescient of their mature function. *Cereb. Cortex* **18**, 2306-2317. doi:10.1093/cercor/bhm258

Batista-Brito, R., Close, J., Machold, R. and Fishell, G. (2008b). The distinct temporal origins of olfactory bulb interneuron subtypes. *J. Neurosci.* **28**, 3966-3975. doi:10.1523/JNEUROSCI.5625-07.2008

Batista-Brito, R., Rossignol, E., Hjerling-Leffler, J., Denaxa, M., Wegner, M., Lefebvre, V., Pachnis, V. and Fishell, G. (2009). The cell-intrinsic requirement of Sox6 for cortical interneuron development. *Neuron* **63**, 466-481. doi:10.1016/j.neuron.2009.08.005

Beclin, C., Follert, P., Stappers, E., Barral, S., Coré, N., de Chevigny, A., Magnone, V., Lebrigand, K., Bissels, U., Huylebroeck, D. et al. (2016). MiR-200 family controls late steps of postnatal forebrain neurogenesis via Zeb2 inhibition. *Sci. Rep.* **6**, 35729. doi:10.1038/srep35729

DEVELOPMENT

Bjornsson, C. S., Apostolopoulou, M., Tian, Y. and Temple, S. (2015). It takes a village: constructing the neurogenic niche. *Dev. Cell* **32**, 435-446. doi:10.1016/j.devcel.2015.01.010

Blanchart, A., De Carlos, J. A. and López-Mascaraque, L. (2006). Time frame of mitral cell development in the mice olfactory bulb. *J. Comp. Neurol.* **496**, 529-543. doi:10.1002/cne.20941

Brill, M. S., Ninkovic, J., Winpenny, E., Hodge, R. D., Ozen, I., Yang, R., Lepier, A., Gascón, S., Erdelyi, F., Szabo, G. et al. (2010). Adult generation of glutamatergic olfactory bulb interneurons. *Nat. Neurosci.* **12**, 1524-1533. doi:10.1038/nn.2416

Cacheux, V., Dastot-Le Moal, F., Kääriäinen, H., Bondurand, N., Rintala, R., Boissier, B., Wilson, M., Mowat, D. and Goossens, M. (2001). Loss-of-function mutations in SIP1 Smad interacting protein 1 result in a syndromic Hirschsprung disease. *Hum. Mol. Genet.* **10**, 1503-1510. doi:10.1093/hmg/10.14.1503

Chng, Z., Teo, A., Pedersen, R. A. and Vallier, L. (2010). SIP1 mediates cell-fate decisions between neuroectoderm and mesendoderm in human pluripotent stem cells. *Cell Stem Cell* **6**, 59-70. doi:10.1016/j.stem.2009.11.015

Chung, D.-W. D., Frausto, R. F., Ann, L. B., Jang, M. S. and Aldave, A. J. (2014). Functional impact of *ZEB1* mutations associated with Posterior Polymorphous and Fuchs' endothelial corneal dystrophies. *Invest. Ophthalmol. Vis. Sci.* **55**, 6159-6166. doi:10.1167/iovs.14-15247

Colak, D., Mori, T., Brill, M. S., Pfeifer, A., Falk, S., Deng, C., Monteiro, R., Mummery, C., Sommer, L. and Gotz, M. (2008). Adult neurogenesis requires Smad4-mediated bone morphogenic protein signaling in stem cells. *J. Neurosci.* **28**, 434-446. doi:10.1523/JNEUROSCI.4374-07.2008

Conidi, A., Cazzola, S., Beets, K., Coddens, K., Collart, C., Cornelis, F., Cox, L., Joke, D., Dobreva, M. P., Dries, R. et al. (2011). Few Smad proteins and many Smad-interacting proteins yield multiple functions and action modes in TGFβ/BMP signaling in vivo. *Cytokine Growth Factor. Rev.* **22**, 287-300. doi:10.1016/j.cytogfr.2011.11.006

Conidi, A., van den Berghe, V., Leslie, K., Stryjewska, A., Xue, H., Chen, Y.-G., Seuntjens, E. and Huylebroeck, D. (2013). Four amino acids within a tandem QxVx repeat in a predicted extended α-helix of the Smad-Binding Domain of Sip1 are necessary for binding to activated Smad proteins. *PLoS ONE* **8**, e76733. doi:10.1371/journal.pone.0076733

Corotto, F. S., Henegar, J. R. and Maruniak, J. A. (1994). Odor deprivation leads to reduced neurogenesis and reduced neuronal survival in the olfactory bulb of the adult mouse. *Neuroscience* **61**, 739-744. doi:10.1016/0306-4522(94)90397-2

Díaz-Guerra, E., Pignatelli, J., Nieto-Estévez, V. and Vicario-Abejón, C. (2013). Transcriptional regulation of olfactory bulb neurogenesis. *Anat. Rec.* **296**, 1364-1382. doi:10.1002/ar.22733

Doetsch, F. and Alvarez-Buylla, A. (1996). Network of tangential pathways for neuronal migration in adult mammalian brain. *Proc. Natl Acad. Sci. USA* **93**, 14895-14900. doi:10.1073/pnas.93.25.14895

Doetsch, F., García-Verdugo, J. M. and Alvarez-Buylla, A. (1997). Cellular composition and three-dimensional organization of the subventricular germinal zone in the adult mammalian brain. *J. Neurosci.* **17**, 5046-5061. doi:10.1523/JNEUROSCI.17-13-05046.1997

Epifanova, E., Babaev, A., Newman, A. G. and Tarabykin, V. (2019). Role of Zeb2/Sip1 in neuronal development. *Brain Res.* **1705**, 24-31. doi:10.1016/j.brainres.2018.09.034

Figueres-Oñate, M. and López-Mascaraque, L. (2016). Adult olfactory bulb interneuron phenotypes identified by targeting embryonic and postnatal neural progenitors. *Front. Neurosci.* **10**, 194. doi:10.3389/fnins.2016.00194

Fogarty, M., Grist, M., Gelman, D., Marin, O., Pachnis, V. and Kessaris, N. (2007). Spatial genetic patterning of the embryonic neuroepithelium generates GABAergic interneuron diversity in the adult cortex. *J. Neurosci.* **27**, 10935-10946. doi:10.1523/JNEUROSCI.1629-07.2007

Fuentealba, L. C., Rompani, S. B., Parraguez, J. I., Obernier, K., Romero, R., Cepko, C. L. and Alvarez-Buylla, A. (2015). Embryonic origin of postnatal neural stem cells. *Cell* **161**, 1644-1655. doi:10.1016/j.cell.2015.05.041

Funahashi, J.-I., Kamachi, Y., Goto, K. and Kondoh, H. (1991). Identification of nuclear factor δEF1 and its binding site essential for lens-specific activity of the δ1-crystallin enhancer. *Nucleic Acids Res.* **19**, 3543-3547. doi:10.1093/nar/19.13.3543

Garavelli, L. and Mainardi, P. C. (2007). Mowat-Wilson Syndrome. *Orphanet J. Rare* **2**, 42. doi:10.1186/1750-1172-2-42

Garavelli, L., Zollino, M., Mainardi, P. C., Gurrieri, F., Rivieri, F., Soli, F., Verri, R., Albertini, E., Favaron, E., Zignani, M. et al. (2009). Mowat-Wilson syndrome: facial phenotype changing with age: study of 19 Italian patients and review of the literature. *Am. J. Med. Genet. A* **149A**, 417-426. doi:10.1002/ajmg.a.32693

Goossens, S., Janzen, V., Bartunkova, S., Yokomizo, T., Drogat, B., Crisan, M., Haigh, K., Seuntjens, E., Umans, L., Riedt, T. et al. (2011). The EMT regulator Zeb2/Sip1 is essential for murine embryonic hematopoietic stem/progenitor cell differentiation and mobilization. *Blood* **117**, 5620-5630. doi:10.1182/blood-2010-08-300236

Gregory-Evans, C. Y., Vieira, H., Dalton, R., Adams, G. G. W., Salt, A. and Gregory-Evans, K. (2004). Ocular coloboma and high myopia with Hirschsprung disease associated with a novel ZFHX1B missense mutation and trisomy 21. *Am. J. Med. Genet.* **131A**, 86-90. doi:10.1002/ajmg.a.30312

Grotewold, L. and Rüther, U. (2002). The Wnt antagonist Dickkopf-1 is regulated by Bmp signaling and c-Jun and modulates programmed cell death. *EMBO J.* **21**, 966-975. doi:10.1093/emboj/21.5.966

Hack, I., Bancila, M., Loulier, K., Carroll, P. and Cremer, H. (2002). Reelin is a detachment signal in tangential chain-migration during postnatal neurogenesis. *Nat. Neurosci.* **5**, 939-945. doi:10.1038/nn923

Hegarty, S. V., Sullivan, A. M. and O'Keeffe, G. W. (2015). Zeb2: a multifunctional regulator of nervous system development. *Prog. Neurobiol.* **132**, 81-95. doi:10.1016/j.pneurobio.2015.07.001

Hegarty, S. V., Wyatt, S. L., Howard, L., Stappers, E., Huylebroeck, D., Sullivan, A. M. and O'Keeffe, G. W. (2017). Zeb2 is a negative regulator of midbrain dopaminergic axon growth and target innervation. *Sci. Rep.* **7**, 8568. doi:10.1038/s41598-017-08900-3

Heinritz, W., Zweier, C., Froster, U. G., Strenge, S., Kujat, A., Syrbe, S., Rauch, A. and Schuster, V. (2006). A Missense mutation in the ZFHX1B gene associated with an atypical Mowat–Wilson syndrome phenotype. *Am. J. Med. Genet.* **140A**, 1223-1227. doi:10.1002/ajmg.a.31267

Higashi, Y., Maruhashi, M., Nelles, L., Van de Putte, T., Verschueren, K., Miyoshi, T., Yoshimoto, A., Kondoh, H. and Huylebroeck, D. (2002). Generation of the floxed allele of the SIP1 (Smad-Interacting Protein 1) gene for Cre-mediated conditional knockout in the mouse. *Genesis* **32**, 82-84. doi:10.1002/gene.10048

Ivanovski, I., Djuric, O., Caraffi, S. G., Santodirocco, D., Pollazzon, M., Rosato, S., Cordelli, D. M., Abdalla, E., Accorsi, P., Adam, M. P. et al. (2018). Phenotype and genotype of 87 patients with Mowat–Wilson syndrome and recommendations for care. *Genet. Med.* **20**, 965-975. doi:10.1038/gim.2017.221

Kawaguchi-Niida, M., Shibata, N. and Furuta, Y. (2017). Smad4 is essential for directional progression from committed neural progenitor cells through neuronal differentiation in the postnatal mouse brain. *Mol. Cell. Neurosci.* **83**, 55-64. doi:10.1016/j.mcn.2017.06.008

Kessaris, N., Fogarty, M., Iannarelli, P., Grist, M., Wegner, M. and Richardson, W. D. (2006). Competing waves of oligodendrocytes in the forebrain and postnatal elimination of an embryonic lineage. *Nat. Neurosci.* **9**, 173-179. doi:10.1038/nn1620

Kosaka, K., Toida, K., Aika, Y. and Kosaka, T. (1998). How simple is the organization of the olfactory glomerulus?: the heterogeneity of so-called periglomerular cells. *Neurosci. Res.* **30**, 101-110. doi:10.1016/S0168-0102(98)00002-9

Kriegstein, A. and Alvarez-Buylla, A. (2009). The glial nature of embryonic and adult neural stem cells. *Annu. Rev. Neurosci.* **32**, 149-184. doi:10.1146/annurev.neuro.051508.135600

Lemasson, M., Saghatelyan, A. and Lledo, P. (2005). Neonatal and adult neurogenesis provide two distinct populations of newborn neurons to the mouse olfactory bulb. *Science* **25**, 6816-6825. doi:10.1523/JNEUROSCI.1114-05.2005

Li, J., Wang, C., Zhang, Z., Wen, Y., An, L., Liang, Q., Xu, Z., Wei, S., Li, W., Guo, T. et al. (2018). Transcription factors Sp8 and Sp9 coordinately regulate olfactory bulb interneuron development. *Cereb. Cortex* **28**, 3278-3294. doi:10.1093/cercor/bhx199

Lim, D. A. and Alvarez-Buylla, A. (2014). Adult neural stem cells stake their ground. *Trends Neurosci.* **37**, 563-571. doi:10.1016/j.tins.2014.08.006

Lim, D. A. and Alvarez-Buylla, A. (2016). The Adult Ventricular–Subventricular Zone (V-SVZ) and Olfactory Bulb (OB) neurogenesis. *Cold Spring Harb. Perspect. Biol.* **8**, a18820. doi:10.1101/cshperspect.a018820

McKinsey, G. L., Lindtner, S., Trzcinski, B., Visel, A., Pennacchio, L. A., Huylebroeck, D., Higashi, Y. and Rubenstein, J. L. R. (2013). Dlx1&2-dependent expression of Zfhx1b (Sip1, Zeb2) regulates the fate switch between cortical and striatal interneurons. *Neuron* **77**, 83-98. doi:10.1016/j.neuron.2012.11.035

Megason, S. G. and McMahon, A. P. (2002). A mitogen gradient of dorsal midline Wnts organizes growth in the CNS. *Development* **129**, 2087-2098.

Merkle, F. T., Fuentealba, L. C., Sanders, T. A., Magno, L., Kessaris, N. and Alvarez-Buylla, A. (2014). Adult neural stem cells in distinct microdomains generate previously unknown interneuron types. *Nat. Neurosci.* **17**, 207-214. doi:10.1038/nn.3610

Miquelajauregui, A., Van de Putte, T., Polyakov, A., Nityanandam, A., Boppana, S., Seuntjens, E., Karabinos, A., Higashi, Y., Huylebroeck, D. and Tarabykin, V. (2007). Smad-interacting protein-1 (Zfhx1b) acts upstream of Wnt signaling in the mouse hippocampus and controls its formation. *Proc. Natl. Acad. Sci. USA* **104**, 12919-12924. doi:10.1073/pnas.0609863104

Mirzadeh, Z., Merkle, F. T., Soriano-Navarro, M., Garcia-Verdugo, J. M. and Alvarez-Buylla, A. (2008). Neural stem cells confer unique pinwheel architecture to the ventricular surface in neurogenic regions of the adult brain. *Cell Stem Cell* **3**, 265-278. doi:10.1016/j.stem.2008.07.004

Mowat, D. R., Croaker, G. D., Cass, D. T., Kerr, B. A., Chaitow, J., Ades, L. C., Chia, N. L. and Wilson, M. J. (1998). Hirschsprung disease, microcephaly, mental retardation, and characteristic facial features: delineation of a new syndrome and identification of a locus at chromosome 2q22-q23. *J. Med. Genet.* **35**, 617-623. doi:10.1136/jmg.35.8.617

Okuyama-Yamamoto, A., Yamamoto, T., Miki, A. and Terashima, T. (2005). Changes in reelin expression in the mouse olfactory bulb after chemical lesion to

the olfactory epithelium. *Eur. J. Neurosci.* **21**, 2586-2592. doi:10.1111/j.1460-9568.2005.04082.x

Omilusik, K. D., Best, J. A., Yu, B., Goossens, S., Weidemann, A., Nguyen, J. V., Seuntjens, E., Stryjewska, A., Zweier, C., Roychoudhuri, R. et al. (2015). Transcriptional repressor ZEB2 promotes terminal differentiation of CD8+ effector and memory T cell populations during infection. *J. Exp. Med.* **212**, 2027-2039. doi:10.1084/jem.20150194

Panman, L., Papathanou, M., Laguna, A., Oosterveen, T., Volakakis, N., Acampora, D., Kurtsdotter, I., Yoshitake, T., Kehr, J., Joodmardi, E. et al. (2014). Sox6 and Otx2 control the specification of substantia nigra and ventral tegmental area dopamine neurons. *Cell Reports* **8**, 1018-1025. doi:10.1016/j.celrep.2014.07.016

Parthasarathy, S., Srivatsa, S., Nityanandam, A. and Tarabykin, V. (2014). Ntf3 acts downstream of Sip1 in cortical postmitotic neurons to control progenitor cell fate through feedback signaling. *Development* **141**, 3324-3330. doi:10.1242/dev.114173

Petreanu, L. and Alvarez-Buylla, A. (2002). Maturation and death of adult-born olfactory bulb granule neurons: role of olfaction. *J. Neurosci.* **22**, 6106-6113. doi:10.1523/JNEUROSCI.22-14-06106.2002

Price, J. L. and Powell, T. P. (1970). The morphology of the granule cells of the olfactory bulb. *J. Cell Sci.* **7**, 91-123.

Qi, S., Song, Y., Peng, Y., Wang, H., Long, H., Yu, X., Li, Z., Fang, L., Wu, A., Luo, W. et al. (2012). ZEB2 mediates multiple pathways regulating cell proliferation, migration, invasion, and apoptosis in glioma. *PLoS ONE* **7**, e38842. doi:10.1371/journal.pone.0038842

Quintes, S., Brinkmann, B. G., Ebert, M., Fröb, F., Kungl, T., Arlt, F. A., Tarabykin, V., Huylebroeck, D., Meijer, D., Suter, U. et al. (2016). Zeb2 is essential for Schwann cell differentiation, myelination and nerve repair. *Nat. Neurosci.* **19**, 1050-1059. doi:10.1038/nn.4321

Remacle, J. E., Kraft, H., Lerchner, W., Wuytens, G., Collart, C., Verschueren, K., Smith, J. C. and Huylebroeck, D. (1999). New mode of DNA binding of multi-zinc finger transcription factors: deltaEF1 family members bind with two hands to two target sites. *EMBO J.* **18**, 5073-5084. doi:10.1093/emboj/18.18.5073

Rochefort, C., Gheusi, G., Vincent, J.-D. and Lledo, P.-M. (2002). Enriched odor exposure increases the number of newborn neurons in the adult olfactory bulb and improves odor memory. *J. Neurosci.* **22**, 2679-2689. doi:10.1523/JNEUROSCI.22-07-02679.2002

Rueden, C. T., Schindelin, J., Hiner, M. C., DeZonia, B. E., Walter, A. E., Arena, E. T. and Eliceiri, K. W. (2017). ImageJ2: ImageJ for the next generation of scientific image data. *BMC Bioinformatics* **18**, 529. doi:10.1186/s12859-017-1934-z

Sayan, A. E., Griffiths, T. R., Pal, R., Browne, G. J., Ruddick, A., Yagci, T., Edwards, R., Mayer, N. J., Qazi, H., Goyal, S. et al. (2009). SIP1 protein protects cells from DNA damage-induced apoptosis and has independent prognostic value in bladder cancer. *Proc. Natl. Acad. Sci. USA* **106**, 14884-14889. doi:10.1073/pnas.0902042106

Schindelin, J., Arganda-Carreras, I., Frise, E., Kaynig, V., Longair, M., Pietzsch, T., Preibisch, S., Rueden, C., Saalfeld, S., Schmid, B. et al. (2012). Fiji: an open-source platform for biological-image analysis. *Nat. Methods* **9**, 676-682. doi:10.1038/nmeth.2019

Scott, C. L., Soen, B., Martens, L., Skrypek, N., Saelens, W., Taminau, J., Blancke, G., Van Isterdael, G., Huylebroeck, D., Haigh, J. et al. (2016). The transcription factor Zeb2 regulates development of conventional and plasmacytoid DCs by repressing Id2. *J. Exp. Med.* **213**, 897-911. doi:10.1084/jem.20151715

Sekido, R., Murai, K., Funahashi, J., Kamachi, Y., Fujisawa-Sehara, A., Nabeshima, Y. and Kondoh, H. (1994). The delta-crystallin enhancer-binding protein delta EF1 is a repressor of E2-box-mediated gene activation. *Mol. Cell. Biol.* **14**, 5692-5700. doi:10.1128/MCB.14.9.5692

Seuntjens, E., Nityanandam, A., Miquelajauregui, A., Debruyn, J., Stryjewska, A., Goebbels, S., Nave, K.-A., Huylebroeck, D. and Tarabykin, V. (2009). Sip1 regulates sequential fate decisions by feedback signaling from postmitotic neurons to progenitors. *Nat. Neurosci.* **12**, 1373-1380. doi:10.1038/nn.2409

Sharov, A. A., Weiner, L., Sharova, T. Y., Siebenhaar, F., Atoyan, R., Reginato, A. M., McNamara, C. A., Funa, K., Gilchrest, B. A. and Brissette, J. L. et al. (2003). Noggin overexpression inhibits eyelid opening by altering epidermal apoptosis and differentiation. *EMBO J.* **22**, 2992-3003. doi:10.1093/emboj/cdg291

Sousa, V. H., Miyoshi, G., Hjerling-Leffler, J., Karayannis, T. and Fishell, G. (2009). Characterization of Nkx6-2-derived neocortical interneuron lineages. *Cereb. Cortex* **19**, i1-i10. doi:10.1093/cercor/bhp038

Srivatsa, S., Parthasarathy, S., Molnár, Z. and Tarabykin, V. (2015). Sip1 downstream effector ninein controls neocortical axonal growth, ipsilateral branching, and microtubule growth and stability. *Neuron* **85**, 998-1012. doi:10.1016/j.neuron.2015.01.018

Stenman, J., Toresson, H. and Campbell, K. (2003). Identification of two distinct progenitor populations in the lateral ganglionic eminence: implications for striatal and olfactory bulb neurogenesis. *J. Neurosci.* **23**, 167-174. doi:10.1523/JNEUROSCI.23-01-00167.2003

Stryjewska, A. (2016). The role of Zeb2 in cell fate decisions during development. *PhD thesis*, KU Leuven, Leuven, Belgium.

Stryjewska, A., Dries, R., Pieters, T., Verstappen, G., Conidi, A., Coddens, K., Francis, A., Umans, L., van IJcken, W. F. J., Berx, G. et al. (2017). Zeb2 regulates cell fate at the exit from epiblast state in mouse embryonic stem cells. *Stem Cells* **35**, 611-625. doi:10.1002/stem.2521

Takahashi, H., Ogawa, Y., Yoshihara, S.-I., Asahina, R., Kinoshita, M., Kitano, T., Kitsuki, M., Tatsumi, K., Okuda, M., Tatsumi, K. et al. (2016). A subtype of olfactory bulb interneurons is required for odor detection and discrimination behaviors. *J. Neurosci.* **36**, 8210-8227. doi:10.1523/JNEUROSCI.2783-15.2016

ten Dijke, P. and Heldin, C.-H. (ed.) (2006). *Smad Signal Transduction. Smads in Proliferation, Differentiation and Disease*. Springer.doi:10.1007/1-4020-4709-6

Urbán, N. and Guillemot, F. (2014). Neurogenesis in the embryonic and adult brain: same regulators, different roles. *Front. Cell. Neurosci.* **8**, 1-19. doi:10.3389/fncel.2014.00396

van den Berghe, V., Stappers, E., Vandesande, B., Dimidschstein, J., Kroes, R., Francis, A., Conidi, A., Lesage, F., Dries, R., Cazzola, S. et al. (2013). Directed migration of cortical interneurons depends on the cell-autonomous action of Sip1. *Neuron* **77**, 70-82. doi:10.1016/j.neuron.2012.11.009

Van Grunsven, L. A., Schellens, A., Huylebroeck, D. and Verschueren, K. (2001). SIP1 (Smad interacting protein 1) and delta EF1 (detla-Crystallin Enhancer Binding Factor) are structurally similar transcription repressors. *J. Bone Joint Surg.* **83**, 40-47. doi:10.2106/00004623-200100001-00006

Van Grunsven, L. A., Michiels, C., Van de Putte, T., Nelles, L., Wuytens, G., Verschueren, K. and Huylebroeck, D. (2003). Interaction between Smad-interacting protein-1 and the corepressor C-terminal binding protein is dispensable for transcriptional repression of E-cadherin. *J. Biol. Chem.* **278**, 26135-26145. doi:10.1074/jbc.M300597200

van Grunsven, L. A., Taelman, V., Michiels, C., Verstappen, G., Souopgui, J., Nichane, M., Moens, E., Opdecamp, K., Vanhomwegen, J., Kricha, S. et al. (2007). XSip1 neuralizing activity involves the co-repressor CtBP and occurs through BMP dependent and independent mechanisms. *Dev. Biol.* **306**, 34-49. doi:10.1016/j.ydbio.2007.02.045

van Helden, M. J., Goossens, S., Daussy, C., Mathieu, A.-L., Faure, F., Marçais, A., Vandamme, N., Farla, N., Mayol, K., Viel, S. et al. (2015). Terminal NK cell maturation is controlled by concerted actions of T-bet and Zeb2 and is essential for melanoma rejection. *J. Exp. Med.* **212**, 2015-2025. doi:10.1084/jem.20150809

Verschueren, K., Remacle, J. E., Collart, C., Kraft, H., Baker, B. S., Tylzanowski, P., Nelles, L., Wuytens, G., Su, M.-T., Bodmer, R. et al. (1999). SIP1, a novel zinc finger/homeodomain repressor, interacts with Smad proteins and binds to 5′-CACCT sequences in candidate target genes. *J. Biol. Chem.* **274**, 20489-20498. doi:10.1074/jbc.274.29.20489

Verstappen, G., van Grunsven, L. A., Michiels, C., Van de Putte, T., Souopgui, J., Van Damme, J., Bellefroid, E., Vandekerckhove, J. and Huylebroeck, D. (2008). Atypical Mowat-Wilson patient confirms the importance of the novel association between ZFHX1B/SIP1 and NuRD corepressor complex. *Hum. Mol. Genet.* **17**, 1175-1183. doi:10.1093/hmg/ddn007

Waclaw, R. R., Allen, Z. J., Bell, S. M., Erdélyi, F., Szabó, G., Potter, S. S. and Campbell, K. (2006). The zinc finger transcription factor Sp8 regulates the generation and diversity of olfactory bulb interneurons. *Neuron* **49**, 503-516. doi:10.1016/j.neuron.2006.01.018

Wakamatsu, N., Yamada, Y., Yamada, K., Ono, T., Nomura, N., Taniguchi, H., Kitoh, H., Mutoh, N., Yamanaka, T., Mushiake, K. et al. (2001). Mutations in SIP1, encoding Smad interacting protein-1, cause a form of Hirschsprung disease. *Nat. Genet.* **27**, 369-370. doi:10.1038/86860

Wei, W., Liu, B., Jiang, H., Jin, K. and Xiang, M. (2019). Requirement of the Mowat-Wilson Syndrome gene *Zeb2* in the differentiation and maintenance of non-photoreceptor cell types during retinal development. *Mol. Neurobiol.* **56**, 1719-1736. doi:10.1007/s12035-018-1186-6

Weng, Q., Chen, Y., Wang, H., Xu, X., Yang, B., He, Q., Shou, W., Chen, Y., Higashi, Y., van den Berghe, V. et al. (2012). Dual-mode modulation of Smad signaling by Smad-interacting protein Sip1 is required for myelination in the central nervous system. *Neuron* **73**, 713-728. doi:10.1016/j.neuron.2011.12.021

Winner, B., Cooper-Kuhn, C. M., Aigner, R., Winkler, J. and Kuhn, H. G. (2002). Long-term survival and cell death of newly generated neurons in the adult rat olfactory bulb. *Eur. J. Neurosci.* **16**, 1681-1689. doi:10.1046/j.1460-9568.2002.02238.x

Wu, L. M. N., Wang, J., Conidi, A., Zhao, C., Wang, H., Ford, Z., Zhang, L., Zweier, C., Ayee, B. G., Maurel, P. et al. (2016). Zeb2 recruits HDAC-NuRD to inhibit notch and controls Schwann cell differentiation and Remyelination. *Nat. Neurosci.* **19**, 1060-1072. doi:10.1038/nn.4322

Yoneda, M., Fujita, T., Yamada, Y., Yamada, K., Fujii, A., Inagaki, T., Nakagawa, H., Shimada, A., Kishikawa, M., Nagaya, M. et al. (2002). Late infantile Hirschsprung disease-mental retardation syndrome with a 3-bp deletion in ZFHX1B. *Neurology* **59**, 1637-1640. doi:10.1212/01.WNL.0000034842.78350.4E

Yoshihara, S.-I., Takahashi, H., Nishimura, N., Naritsuka, H., Shirao, T., Hirai, H., Yoshihara, Y., Mori, K., Stern, P. L. and Tsuboi, A. (2012). 5T4 glycoprotein regulates the sensory input-dependent development of a specific subtype of newborn interneurons in the mouse olfactory bulb. *J. Neurosci.* **32**, 2217-2226. doi:10.1523/JNEUROSCI.5907-11.2012

DEVELOPMENT

Young, K. M., Fogarty, M., Kessaris, N. and Richardson, W. D. (2007). Subventricular zone stem cells are heterogeneous with respect to their embryonic origins and neurogenic fates in the adult olfactory bulb. *J. Neurosci.* **27**, 8286-8296. doi:10.1523/JNEUROSCI.0476-07.2007

Zweier, C., Albrecht, B., Mitulla, B., Behrens, R., Beese, M., Gillessen-Kaesbach, G., Rott, H.-D. and Rauch, A. (2002). "Mowat-Wilson" syndrome with and without Hirschsprung disease is a distinct, recognizable multiple congenital anomalies-mental retardation syndrome caused by mutations in the zinc finger homeo box 1B gene. *Am. J. Med. Genet.* **108**, 177-181. doi:10.1002/ajmg.10226

Zweier, C., Thiel, C. T., Dufke, A., Crow, Y. J., Meinecke, P., Suri, M., Ala-Mello, S., Beemer, F., Bernasconi, S., Bianchi, P. et al. (2005). Clinical and mutational spectrum of Mowat-Wilson Syndrome. *Eur. J. Med. Genet.* **48**, 97-111. doi:10.1016/j.ejmg.2005.01.003

Zweier, C., Hord, D., Kraus, C. and Rauch, A. (2006). Atypical ZFHX1B mutation associated with a mild Mowat-Wilson syndrome phenotype. *Am. J. Med. Genet.* **140**, 869-872. doi:10.1002/ajmg.a

DEVELOPMENT